Title

Effects of Pore and Cage Topology on the Thermodynamics of n-Alkane Adsorption at Brønsted Protons in Zeolites at High Temperature

Journal

The Journal of Physical Chemistry C, 121(3)

ISSN

1932-7447

Authors

Janda, Amber
Vlaisavljevich, Bess
Smit, Berend
et al.

Publication Date

2017-01-26

DOI

10.1021/acs.jpcc.6b09703

Peer reviewed

THE JOURNAL OF PHYSICAL CHEMISTRY C

Article

pubs.acs.org/JPCC

Effects of Pore and Cage Topology on the Thermodynamics of *n*-Alkane Adsorption at Brønsted Protons in Zeolites at High Temperature

Amber Janda,[†,⊥] Bess Vlaisavljevich,[‡] Berend Smit,[†,§] Li-Chiang Lin,[*,∥] and Alexis T. Bell[*,†]

[†]Department of Chemical and Biomolecular Engineering, University of California, Berkeley, Berkeley, California 94720, United States

[‡]Department of Chemistry, Northwestern University, 2145 Sheridan Road, Evanston, Illinois 60208, United States

[§]Institute of Chemical Sciences and Engineering, École Polytechnique Fédérale de Lausanne, Rue de l'Industrie 17, CH-1951 Sion, Switzerland

[∥]William G. Lowrie Department of Chemical and Biomolecular Engineering, The Ohio State University, 151 West Woodruff Avenue, Columbus, Ohio 43210, United States

Supporting Information

ABSTRACT: Monte Carlo simulations are used to systematically investigate the effects of structural topology on the thermodynamics of *n*-alkanes adsorbed at Brønsted protons in zeolites having one-dimensional channel systems. In zeolites without cages, the enthalpy and entropy of adsorption ($\Delta H_{ads\text{-}H^+}$ and $\Delta S_{ads\text{-}H^+}$) at fixed pore-limiting diameter (PLD) generally increase (become less negative) as the ratio of the minimum to maximum channel diameter decreases, and are lowest when this ratio equals 1 (corresponding to approximately circular cross sections). The effect of a change in diameter ratio on the free energy of adsorption ($\Delta A_{ads\text{-}H^+}$) is weak because the changes in $\Delta H_{ads\text{-}H^+}$ and $T\Delta S_{ads\text{-}H^+}$ largely cancel. The addition of cages having a largest-cavity diameter (LCD) greater than the PLD increases both $\Delta H_{ads\text{-}H^+}$ and $\Delta S_{ads\text{-}H^+}$. Replacing channels with cages of the same diameter does not change $\Delta S_{ads\text{-}H^+}$ significantly when the PLD is similar to the alkane length but decreases both $\Delta H_{ads\text{-}H^+}$ and $\Delta A_{ads\text{-}H^+}$ because of the greater surface area of cages relative to channels. The selectivity to adsorption via a central C−C bond vs a terminal bond when cages are absent is smallest for PLDs near the alkane length and, when cages are present, is even lower when the LCD exceeds the alkane length. This effect is attributed to more rotation of the alkane in cages vs channels. The results show that $\Delta A_{ads\text{-}H^+}$ at 773 K can be tuned by manipulating a characteristic dimension (LCD, PLD) and topology (e.g., adding cages) simultaneously, in order to circumvent the compensating changes in $T\Delta S_{ads\text{-}H^+}$ and $\Delta H_{ads\text{-}H^+}$ that occur upon changing only one structural parameter.

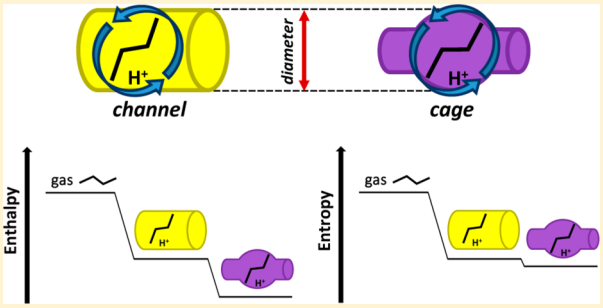

1. INTRODUCTION

Zeolites are microporous aluminosilicates whose shape-selective properties are exploited extensively for the catalytic cracking of hydrocarbons.[1−5] The apparent kinetics of cracking are affected by the thermodynamics and kinetics of hydrocarbon adsorption, which are in turn affected by zeolite topology. For these reasons, many previous studies have been aimed at elucidating the effects of topology on adsorption behavior.[6−12] Transformations of hydrocarbons are often carried out at high pressures and surface coverages and are limited by diffusion. However, Monte Carlo simulations of equilibrium adsorption, both at high coverages[7] and even in the Henry region,[6] have been successfully used to rationalize observed selectivities for processes including hydrocracking and dewaxing.[12−15] Since the Henry region also corresponds to conditions approaching zero coverage, adsorption behavior in this region reflects the intrinsic effects of the zeolite topology.

Considering the usefulness of the Henry region for predicting reaction selectivities, it is of interest to understand how zeolite topology affects adsorption thermodynamics in this region and how topology could, therefore, be manipulated to tune adsorption behavior. Several studies have been focused on measuring[16−18] or computing[19−22] thermodynamic adsorption properties for alkane adsorption and then interpreting the results based on a qualitative assessment of the level of confinement. Lower (i.e., more negative) values for the enthalpies and entropies of adsorption are generally associated with more confining features such as small pores, while higher values are associated with less confining features such as large cages. In other work, the observed thermodynamic properties have been rationalized on the basis of the match in shape between the alkane and a zeolite structural feature. Denayer et al.[23,24] have reported that adsorption of alkane isomers of a given carbon number in MWW is more favorable for isomers with a gas-phase

Received: September 25, 2016
Revised: December 18, 2016
Published: December 20, 2016

DOI: 10.1021/acs.jpcc.6b09703
J. Phys. Chem. C 2017, 121, 1618−1638

radius of gyration not smaller than that of the cage. For branched isomers having shapes that closely match that of the cage (i.e., isobutane in MWW), adsorption is also thermodynamically favorable over the linear isomer even if the gyration radius of the linear isomer is smaller than that of the cage. These results were attributed to the effect of cage size on the rotational freedom of alkanes, and to optimal enthalpic interactions when the shape traced by a freely rotating branched alkane matches that of the cage.

The importance of the match in size between a cage and alkane has also been noted for other zeolites. Several authors[13,14,25] have used configurational-bias Monte Carlo (CBMC) simulations to simulate alkane adsorption in zeolites with cages at ∼600 K and have reported that, when the diameter of the channels (termed "windows") between cages is commensurate with the diameter of an *n*-alkane (∼4.3 Å), alkanes that are short enough to fit within a single cage are adsorbed preferentially over longer alkanes. Adsorption of the longer alkanes is disfavored because of repulsive interactions between the alkane and the windows. Zeolites with larger window diameters are less prone to such effects[13,14] because the interactions between the alkane and the windows are attractive for larger diameters. The above studies demonstrate the importance of the size as well as the shape of the channels and cages within zeolites on their ability to adsorb hydrocarbons.

While the above-mentioned studies have involved primarily qualitative interpretations of the effects of zeolite structure on adsorption, a few studies have also attempted to correlate a quantitative descriptor of pore size with the adsorption enthalpy or entropy. Eder and Lercher[26] have reported that the enthalpy of adsorption, measured at ∼340 K for alkanes in several zeolites, generally became less negative with an increase in the "average pore diameter". Similar findings have also been reported by Savitz et al.[27] and by Gribov et al.[28] In addition, Bates et al.[29] have observed that the heat of *n*-alkane adsorption at 298 K, determined using CBMC simulations, decreased with an increase in the mean pore diameter for several commonly used zeolites, although the value of this diameter was specified on the basis of the location most thermodynamically preferred for adsorption within the zeolite. For zeolites with cages and relatively narrow channels (RHO and LTA), the alkanes were found to be located primarily in the cages and, therefore, the cage diameter was used as the characteristic pore size for these zeolites.

The preceding discussion shows that considerable efforts have been made to interpret the influence of zeolite topology on adsorption qualitatively, whereas efforts to correlate structural parameters with thermodynamics have been limited. Knowledge of how structural descriptors affect thermodynamics would enable the rational selection of zeolites for a given application. It should also be noted that the majority of the studies reported in the literature—those that employ Monte Carlo simulations as well as those that employ experimental measurements—have dealt with nonspecific adsorption of alkanes anywhere within the zeolite and do not limit their analysis to adsorption at catalytically active sites (e.g., at Brønsted protons). A difficulty with studying such adsorption experimentally is that it can be done only at sufficiently low temperature, and specific adsorption at protons must be verified spectroscopically. In addition, using quantum chemical calculations to model specific adsorption is limited by current computational methods which do not properly account for the contribution of local rotation and translation to the entropy.[30−32] It is essential to model adsorption at catalytically active sites accurately in order to properly relate the structure of a zeolite to its activity and selectivity, as has been shown recently for the monomolecular cracking and dehydrogenation of alkanes.[33,34]

In this work, the effects of channel and cage topology on adsorption thermodynamics for linear alkanes (C3−C6) adsorbed at Brønsted protons within zeolites at 773 K are investigated systematically using Monte Carlo simulations. An advantage of using Monte Carlo simulations is that the simulation accounts for the contributions of rotation and translation to the entropy, discussed above, without the need to choose distances for translation or the degree of free rotation.[35,36] Attention is focused on *n*-butane adsorption within one-dimensional frameworks included in the database of the International Zeolite Association (IZA), and an analysis is carried out of the effects of changes in each structural descriptor on the enthalpy, entropy, and free energy ($\Delta H_{ads\text{-}H^+}$, $\Delta S_{ads\text{-}H^+}$, and $\Delta A_{ads\text{-}H^+}$) of adsorption of butane at a Brønsted-acid site. The influence of these descriptors on the relative probability of *n*-butane adsorption occurring via a central vs a terminal C−C bond (which affects the selectivity of monomolecular cracking) is also investigated.[37] Strategies are suggested for manipulating pore descriptors in order to achieve a change in $\Delta A_{ads\text{-}H^+}$ that minimizes the effects of strongly compensating changes in $\Delta H_{ads\text{-}H^+}$ and $T\Delta S_{ads\text{-}H^+}$ at 773 K.

2. CONFIGURATIONAL-BIAS MONTE CARLO SIMULATIONS

The Widom test particle insertion method[38] was used, as described in ref 34, to compute the Henry coefficient (K_H) and the enthalpy of adsorption (ΔH_{ads}, corresponding to the ensemble average for adsorption of alkane anywhere within the zeolite pores) for linear alkanes (propane through *n*-hexane) moving from the gas phase into one-dimensional zeolites having one Al atom per unit cell.[33,37,39] In order to account for the specific interaction between the alkane and the Brønsted proton associated with the Al atom, the four O atoms attached to each Al atom were modeled using a single effective potential with force field parameters obtained as described in our previous work.[34] These parameters have been fit in order to reproduce the experimentally measured values of ΔH_{ads} for *n*-alkanes adsorbed in Brønsted-acidic FAU, which has 12-MR pores connecting large cages. Values of ΔH_{ads} for CHA (which has 8-MR pores and smaller cages) calculated independently using this force field were within 0.1−0.3 kJ mol^{-1} of experimental values.[34] Thus, the force field is transferable across a wide range of pore sizes. Several million Widom insertions were carried out to ensure statistically accurate ensemble averages. To avoid insertions occurring within inaccessible pore space, regions of the zeolite that are inaccessible to methane were first identified using Zeo++.[40] When an insertion occurs within the inaccessible regions, the energy of the insertion is set equal to positive infinity, which effectively excludes the configuration. It is noted that not all zeolite structures investigated in this work have been synthesized as aluminosilicates; several structures have other compositions (e.g., aluminophosphate). The focus of this work is to investigate the influence of pore structure on alkane adsorption, and therefore, all structures investigated were composed of Al, Si, and O atoms, with all T atoms treated as Al or Si.

The enthalpy and entropy of adsorption for molecules adsorbed at Brønsted protons were determined from the configurations in which the alkane molecule is in a reactant state, defined as any configuration in which both carbon atoms of a C−C bond *j* are located within 5 Å of an Al atom at T-site *i*.[37]

DOI: 10.1021/acs.jpcc.6b09703
J. Phys. Chem. C 2017, 121, 1618−1638

Each insertion was assigned to the reactant or nonreactant state and given a value of j, where a value of 1 indicates the terminal bond and values of 2, 3, etc., indicate indistinguishable nonterminal bonds in order of their position relative to the terminal bond. Adsorption enthalpies and Henry coefficients for adsorption at Brønsted protons ($\Delta H_{ads\text{-}H^+}(i,j)$ and $K_{H-H^+}(i,j)$) were then determined from the configurations associated with the reactant state, as described in ref 34. The internal energy change of adsorption ($\Delta U_{ads\text{-}H^+}(i,j)$) was computed directly from the ensemble-averaged energies of molecules in the reactant state, and $\Delta H_{ads\text{-}H^+}(i,j)$ was calculated from the equation $\Delta H_{ads\text{-}H^+}(i,j) = \Delta U_{ads\text{-}H^+}(i,j) - RT$.[33]

The entropy of adsorption was obtained using the relationship of $K_{H-H^+}(i,j)$ to the dimensionless thermodynamic equilibrium constant, $K_{ads\text{-}H^+}(i,j)$, which is a natural function of the Helmholtz free energy change for adsorption,[33,41] $\Delta A_{ads\text{-}H^+}$,

$$\frac{RT}{V_{H^+}n_{H^+}}K_{H-H^+}(i,j) \equiv K_{ads\text{-}H^+}(i,j) = \exp\left(-\frac{\Delta A_{ads\text{-}H^+}(i,j)}{RT}\right) \quad (1)$$

where n_{H^+} is the moles of protons per kilogram of zeolite and V_{H^+} is the volume contained in 1 mol of reactant state spheres of radius 5 Å. The Helmholtz free energy change for adsorption is related to $\Delta H_{ads\text{-}H^+}$ and $\Delta S_{ads\text{-}H^+}$ according to $\Delta A_{ads\text{-}H^+} = \Delta H_{ads\text{-}H^+} + RT - T\Delta S_{ads\text{-}H^+}$. The value of $\Delta S_{ads\text{-}H^+}$ was determined by substituting this relationship into eq 1 and rearranging to obtain

$$\Delta S_{ads\text{-}H^+}(i,j) = R\ln\left[\frac{RT}{V_{H^+}n_{H^+}}K_{H-H^+}(i,j)\right] + \frac{\Delta H_{ads\text{-}H^+}(i,j) + RT}{T} \quad (2)$$

It can be seen from eq 2 that K_{H-H^+} (equal to the moles of alkane adsorbed at Brønsted protons per unit mass of zeolite per unit pressure) is normalized by the concentration of protons per unit mass of zeolite (n_{H^+}). In addition, the simulations correspond to infinite dilution conditions. Therefore, there is no configurational contribution to $\Delta S_{ads\text{-}H^+}$ arising from the degenerate arrangements of alkanes over unoccupied sites, and values of $\Delta S_{ads\text{-}H^+}$ can be compared directly between zeolites having different Al atom concentrations at the same temperature. The expected values of $\Delta H_{ads\text{-}H^+}(j)$ and $\Delta S_{ads\text{-}H^+}(j)$ corresponding to a random distribution of Al were taken as the Boltzmann averages of $\Delta H_{ads\text{-}H^+}(i,j)$ and $\Delta S_{ads\text{-}H^+}(i,j)$ over all T-sites i, and the expected values of $\Delta H_{ads\text{-}H^+}$ and $\Delta S_{ads\text{-}H^+}$ for a given alkane were taken as the Boltzmann averages of $\Delta H_{ads\text{-}H^+}(j)$ and $\Delta S_{ads\text{-}H^+}(j)$ over all bonds j. The above methods for determining $\Delta H_{ads\text{-}H^+}$ and $\Delta S_{ads\text{-}H^+}$ have been previously demonstrated to result in good agreement with experimental values for n-alkanes adsorbed within H-MFI.[33] Only zeolites for which $\Delta A_{ads\text{-}H^+}$ at 773 K was less than 15 kJ mol^{-1} for at least one alkane were used to analyze the effects of pore topology because these frameworks are most likely to find practical use.

It is noted that, since zeolites with different frameworks have different numbers of T atoms in their unit cells, the density of Al atoms in the simulations will vary among zeolites. To investigate the effects of Al concentration on adsorption, simulations were run for three zeolites having a range of Al atom concentrations per unit volume (AFI, ATO, and SSY). The cell for each zeolite was then enlarged by a factor of 2−8 (i.e., composed of 2−8 unit cells), thereby increasing the Si/Al ratio of the enlarged cell by the same factor. As shown in the Supporting Information (section S.1), the adsorption properties of n-butane for the single unit cell vs the enlarged cell are quantitatively similar for all three zeolites and differences in adsorption properties do not correlate with the Al concentration in the original cell. The values of $\Delta H_{ads\text{-}H^+}(i)$ and $\Delta S_{ads\text{-}H^+}(i)$ at 773 K determined for each cell were found to be within ∼2 kJ mol^{-1} and ∼1 J mol^{-1} K^{-1}, respectively, for all three zeolites. The ratio of equilibrium constants $K_{ads\text{-}H^+}(j)$ for adsorption to form a central (j = 2) vs a terminal (j = 1) cracking reactant state were within ∼0.02. Differences in thermodynamic parameters among zeolites that exceed these small amounts are caused by differences in framework structure and not by differences in Al concentration, which is sufficiently low to avoid such confounding. The effects of neighboring Al sites on thermodynamics will become significant as the Al concentration increases beyond a critical value. An investigation of the effects of Al concentration on adsorption is beyond the scope of this work, but such effects in zeolites that are naturally rich in Al (e.g., FAU) are pronounced, and are therefore relevant for modeling adsorption. The effects of Al concentration on thermodynamics for alkanes adsorbed in a reactant state, and the implications for simulations of adsorption, will be the subject of a future publication.

To facilitate interpretations of the influence of zeolite structure on adsorption thermodynamics, the locations of alkane C atoms relative to the Al atoms in the zeolite were visualized for several zeolite structures. To obtain data for the visualizations, CBMC simulations were performed in the canonical (NVT) ensemble. A representative T-site was first selected for each zeolite having multiple T-site symmetries. As discussed in the Supporting Information (section S.4), the T-site was chosen such that the thermodynamic properties for adsorption at the T-site (i.e., $\Delta H_{ads\text{-}H^+}(i,j)$) most closely matched the ensemble-averaged properties (i.e., $\Delta H_{ads\text{-}H^+}(j)$). A single n-butane molecule was then placed in the simulation box of the selected zeolite containing one Al atom per unit cell. Eight million MC moves including rotation, translation, and reinsertion were performed, and configurations were collected every 20 moves.

For configurations in which the alkane was found to be in a reactant state, the coordinates of all C atoms in the molecule were recorded. The coordinates of the two C atoms comprising the bond j in the reactant state and the coordinates of the remaining two C atoms were then visualized separately. (It is noted that the two C atoms attached to those comprising the bond j in a reactant state are not necessarily located outside the 5 Å sphere that defines the reactant state.) The locations of each set of C atoms were presented as heat maps by projecting the coordinates of the zeolite and C atoms onto planes parallel to and perpendicular to the channel direction. The color scale of each heat map shows the percentage of coordinates located within square bins of side length 0.06 Å. For ease of viewing, the heat maps were numerically smoothed using the methods developed by Eilers and Goeman[42] with a smoothing parameter (lambda) of 3. More than 5000 C atom coordinates from the NVT simulations are visualized in each heat map.

3. RESULTS AND DISCUSSION

3.1. Effects of Channel Diameter and Cross Section for Zeolites without Cages. The effects of channel topology on adsorption thermodynamics in one-dimensional (1D) zeolites lacking cages are analyzed first. Before proceeding, it is necessary to define the parameters that describe channel topology. Channels can differ among zeolites in dimensions, and in the

DOI: 10.1021/acs.jpcc.6b09703
J. Phys. Chem. C 2017, 121, 1618−1638

shapes of the channel space when viewed parallel and perpendicular to the channel direction. In order to simplify the analysis, only zeolites that possess straight channels are considered in this work. Although previous studies have demonstrated that the shape traced by the channel path (e.g., straight, sinusoidal) influences alkane adsorption behavior,[19−21,43−45] zeolites with channels that do not trace straight paths have been omitted because of their small number in the database. However, even among zeolites having only straight channels, the atoms that comprise the channel openings may connect to form circles, ovals, or other shapes, and these shapes are expected to influence the adsorption thermodynamics.[46,47] While no single parameter can describe differences in cross-sectional shape completely, the degree of asymmetry of the cross section is described in this work using the ratio of the smallest to the largest channel diameter (defined as the diameter ratio) reported in the IZA database. To describe the size of the channels, the pore-limiting diameter (PLD), tabulated in the ZEOMICS database,[48] is used. The PLD defines the maximum diameter of a sphere that can freely traverse the channels.[48]

To show qualitatively how the channel topology differs among zeolites that have different PLDs or diameter ratios, illustrations of channel cross sections viewed perpendicular to the center axis are shown in Figure 1. Figure 1a represents a circular channel

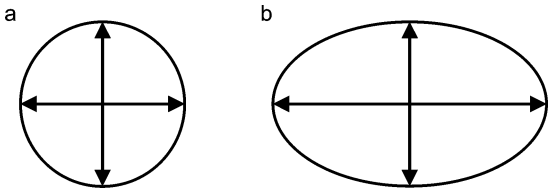

Figure 1. Representation of the cross sections of (a) circular and (b) ovoid channels in zeolites with the same pore-limiting diameter (PLD). For the circular cross sections, the perpendicular arrows, which represent diameters equal to the PLD, are equal in length, while, for the ovoid cross sections, the horizontal arrow is larger than the vertical arrow.

cross section with a diameter ratio of 1. Two diameters (equal to the PLD) are drawn orthogonal to one another and have the same length. Figure 1b shows an oval-shaped cross section for which the vertical diameter is equal to that of the circular channel and the horizontal diameter is longer. It can be seen that the oval-shaped pore has a greater cross-sectional area relative to the pore having a circular cross section of the same PLD. It is noted that, for noncircular channels, the average diameter does not accurately reflect either the minimum or maximum diameter, although in previous studies the average diameter has been used, or one diameter has been chosen and then correlated with measured adsorption properties.[26−29]

The framework types and material names of one-dimensional zeolites that were found to have a Helmholtz free energy of adsorption <15 kJ mol^{-1} at 773 K are listed in Table 1. Included for each zeolite are the number of T atoms that comprise the channel perimeter, the PLD, channel diameters taken from the IZA database, and the ratio of these diameters. It is noted that the PLD does not always lie within the range of the channel diameters taken from the IZA database, likely as a result of differences in the methodologies used to obtain these descriptors. However, the ratio of the diameters—which is anticipated to be less sensitive to methodology than are the individual diameters and PLD—is determined using only the IZA database. Two of the zeolites (MOR and ETR) also have 8-MR side pockets. However, the smallest diameter of the 8-MR pore cross sections (based on IZA-tabulated data) is ∼2.5 Å, and consequently, adsorption at these locations is highly disfavored at 773 K.[30] Therefore, the presence of the pockets is not expected to measurably influence ensemble-averaged adsorption thermodynamics. This conclusion is supported by values of the Henry coefficient that are 2−10 orders of magnitude smaller for adsorption of *n*-butane at side pockets vs main channels for both ETR and MOR (see the Supporting Information, section S.2).

Plots of $\Delta H_{ads\text{-}H^+}$ and $\Delta S_{ads\text{-}H^+}$ at 773 K vs PLD for *n*-butane are presented in Figure 2. The colors of the points indicate the diameter ratio. Triangles correspond to zeolites without side pockets, and diamonds are used to represent MOR and ETR. The data for all plots in this section are included in Table 2. It can be seen that, as the PLD increases, $\Delta H_{ads\text{-}H^+}$ and $\Delta S_{ads\text{-}H^+}$ increase (i.e., become less negative) for a fixed diameter ratio, consistent with previous conclusions that, in general, the enthalpy of adsorption increases with an increase in pore diameter because of a reduction in the strength of van der Waals interactions between the alkane and the zeolite. It can also be seen that, at a fixed PLD, $\Delta H_{ads\text{-}H^+}$ and $\Delta S_{ads\text{-}H^+}$ tend to be higher for zeolites with lower diameter ratios, although for $\Delta S_{ads\text{-}H^+}$ this is observed only for PLDs below 7 Å. This observation suggests that thermodynamics are most sensitive to the cross-sectional shape of the pores when the pore dimensions are on the order of those for *n*-butane (∼4.3 × 8 Å). Within such pores, the interactions between butane and the zeolite will be strongest and the effects of changes in topology on thermodynamics will be commensurately more noticeable than those for larger pores.

The observed effects of the diameter ratio on $\Delta H_{ads\text{-}H^+}$ and $\Delta S_{ads\text{-}H^+}$ can be rationalized by comparing the configurations collected for *n*-butane adsorbed in CAN, which has pores of circular cross section, and in SSY, which has pores with oval cross section. Both zeolites have a PLD of 6.6 Å, while CAN has a diameter ratio of 1.00 and SSY has a diameter ratio of 0.66. Heat maps generated using data taken from NVT simulations and showing the locations of C atoms for *n*-butane in *j*1 (terminal) and *j*2 (central) cracking reactant states are presented in Figures 3 and 4, respectively, for CAN and SSY. The locations of zeolite atoms at the periphery of the channels are shown with circles. It can be seen that, for both types of reactant states, the two C atoms that are in the reactant state, as well as the remaining C atoms, explore a larger area in SSY than in CAN. The C atoms for SSY are also located farther, on average, from zeolite O atoms than in CAN as a consequence of the larger diameter of SSY in the *x* direction (10 Å). Consequently, *n*-butane interacts with the zeolite more weakly in SSY than in CAN, and the values of $\Delta H_{ads\text{-}H^+}$ and $\Delta S_{ads\text{-}H^+}$ are correspondingly higher for SSY (−41.0 kJ mol^{-1}, −52.7 J mol^{-1} K^{-1}) than for CAN (−51.3 kJ mol^{-1}, −59.5 J mol^{-1} K^{-1}).

The impact of PLD and diameter ratio on the Helmholtz free energy of adsorption ($\Delta A_{ads\text{-}H^+} = \Delta H_{ads\text{-}H^+} - T\Delta S_{ads\text{-}H^+} + RT$)[14,37] can be seen in a plot of $\Delta A_{ads\text{-}H^+}$ vs PLD presented in Figure 5. Because the overall trends in $\Delta S_{ads\text{-}H^+}$ and $\Delta H_{ads\text{-}H^+}$ with respect to PLD and diameter ratio are qualitatively similar, and because at 773 K $T\Delta S_{ads\text{-}H^+}$ contributes significantly to $\Delta A_{ads\text{-}H^+}$, the values of $\Delta A_{ads\text{-}H^+}$ fall within a narrower range (∼13 kJ mol^{-1}) compared to $\Delta H_{ads\text{-}H^+}$ (∼40 kJ mol^{-1}). While there is no systematic effect of the diameter ratio on $\Delta A_{ads\text{-}H^+}$ observable in Figure 5, in general, $\Delta A_{ads\text{-}H^+}$ increases with increasing PLD between 6.5 and 12 Å, with the lowest values for $\Delta A_{ads\text{-}H^+}$ appearing mostly between PLDs of 6−7 Å. Thus, the overall change in $\Delta A_{ads\text{-}H^+}$ with PLD

DOI: 10.1021/acs.jpcc.6b09703
J. Phys. Chem. C 2017, 121, 1618−1638

Table 1. IZA Framework Types and Material Names (in Parentheses), Pore-Limiting Diameter (PLD), Channel Diameters, and Ratio of Channel Diameters for One-Dimensional Zeolites

framework type and material name	channel ring size (T atoms)	PLD[b] (Å)	channel diameter[c] (Å)	channel diameter ratio[c] (Å)
AEL (AlPO-11)	10	5.3	4.0 × 6.5	0.62
AET (AlPO-8)	14	8.2	7.9 × 8.7	0.91
AFI (AlPO-5)	12	8.1	7.3 × 7.3	1.00
AFO (AlPO-41)	10	5.6	4.1 × 5.3	0.77
ATO (AlPO-31)	12	6.1	5.4 × 5.4	1.00
ATS (MAPO-36)	12	7.3	6.5 × 7.5	0.87
CAN (Cancrinite)	12	6.6	5.9 × 5.9	1.00
DON (UTD-1F)	14	8.7	8.1 × 8.2	0.99
ETR (ECR-34)[a]	18[a]	10.0	10.1 × 10.1	1.00
IFR (ITQ-4)	12	6.3	6.2 × 7.2	0.86
MOR (Mordenite)[a]	12[a]	6.5	6.5 × 7.0	0.93
MRE (ZSM-48)	10	6.2	5.6 × 5.6	1.00
MTT (ZSM-23)	10	5.7	4.5 × 5.2	0.87
MTW (ZSM-12)	12	6.3	5.6 × 6.0	0.93
OSI (UiO-6)	12	6.9	5.2 × 6.0	0.87
SFE (SSZ-48)	12	6.5	5.4 × 7.6	0.71
SFH (SSZ-53)	14	7.6	6.4 × 8.7	0.74
SFN (SSZ-59)	14	7.3	6.2 × 8.5	0.73
SSY (SSZ-60)	12	6.6	5.0 × 7.6	0.66
STO (SSZ-31 polymorph I)	12	6.7	5.7 × 8.6	0.66
TON (ZSM-22)	10	5.7	4.6 × 5.7	0.81
VET (VPI-8)	12	6.6	5.9 × 5.9	1.00
VFI (VPI-5)	18	12.0	12.7 × 12.7	1.00

[a]ETR and MOR also contain 8-MR side pockets ~2.5 Å along the shorter dimension that are essentially inaccessible at 773 K (see Supporting Information, section S.2).[30] [b]Pore-limiting diameter (PLD) calculated by First et al.[48] [c]Channel diameters taken from the IZA database, and ratio of minimum to maximum diameter.

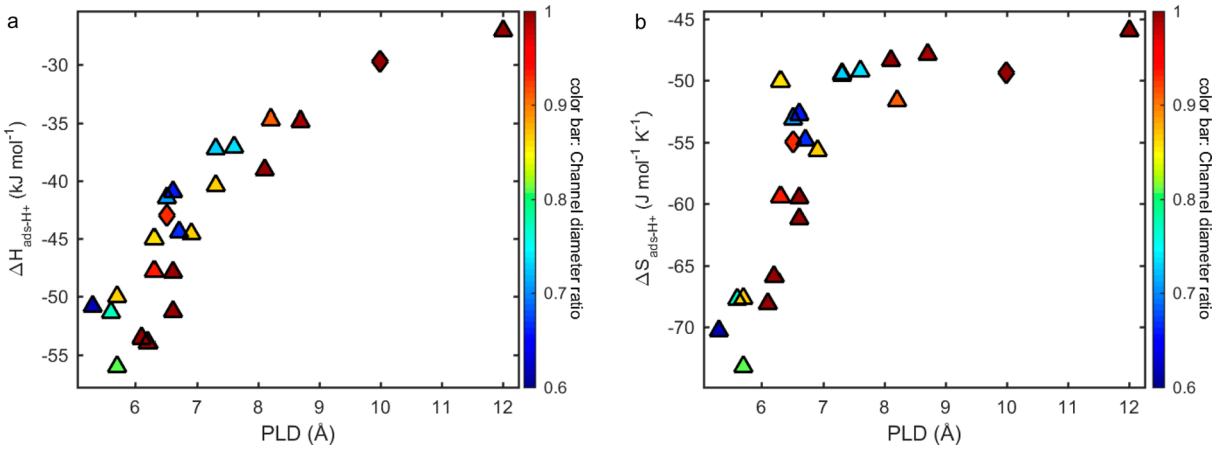

Figure 2. (a) Enthalpy of adsorption and (b) entropy of adsorption at 773 K for *n*-butane adsorbed in a reactant state in one-dimensional zeolites vs the pore-limiting diameter (PLD). Diamonds correspond to zeolites with 8-MR side pockets and triangles to zeolites without side pockets. The color bar indicates the ratio of the minimum to maximum channel width given in Table 2.

reflects primarily the change in $\Delta H_{ads\text{-}H^+}$ except for PLDs below ~6 Å. For PLDs < 6 Å, the decrease in $\Delta S_{ads\text{-}H^+}$ that occurs with a decrease in diameter is accompanied by a smaller gain in enthalpic stabilization relative to PLDs in the optimal range, causing $\Delta A_{ads\text{-}H^+}$ to increase. These results are consistent with previous conclusions[14] that channels less than 4.7 Å in diameter (based on IZA tabulated data) lead to repulsive interactions. Table 1 shows that zeolites with PLDs less than 6 Å in the present work possess one channel width that is less than 4.7 Å based on IZA tabulated data.

In summary, the above results show that, in order to minimize $\Delta A_{ads\text{-}H^+}$ at 773 K for *n*-butane, the PLD must usually be limited to 6−7 Å, because enthalpic interactions with the zeolite are optimized for pores of this diameter. The diameter ratio influences $\Delta H_{ads\text{-}H^+}$ and $\Delta S_{ads\text{-}H^+}$ individually but does not influence $\Delta A_{ads\text{-}H^+}$ systematically at 773 K for the zeolites investigated. As temperature is decreased, it can be expected that the dependence of $\Delta A_{ads\text{-}H^+}$ on structure would increasingly reflect the influence of structure on $\Delta H_{ads\text{-}H^+}$ rather than on $T\Delta S_{ads\text{-}H^+}$, and that at lower temperatures the diameter ratio could also be manipulated to control $\Delta A_{ads\text{-}H^+}$. The enthalpic effects of a change in PLD on $\Delta A_{ads\text{-}H^+}$ would also become more pronounced. At 773 K, however, the compensatory effects of changes in $\Delta H_{ads\text{-}H^+}$ and $T\Delta S_{ads\text{-}H^+}$ with each structural parameter cause some of this control to be lost. Enthalpy−entropy compensation poses a problem for the rational design of

DOI: 10.1021/acs.jpcc.6b09703
J. Phys. Chem. C 2017, 121, 1618−1638

Table 2. Thermodynamic Quantities Obtained Using CBMC Simulations for Adsorption of *n*-Butane at 773 K in One-Dimensional Zeolites Listed in Order of Increasing PLD

framework type	PLD[a] (Å)	diameter ratio[a] (Å)	$\Delta H_{ads\text{-}H^+}$[b] (kJ mol^{-1})	$\Delta S_{ads\text{-}H^+}$[b] (J mol^{-1} K^{-1})	$\Delta A_{ads\text{-}H^+}$[b] (kJ mol^{-1})	$K_{ads\text{-}H^+}(j2)/K_{ads\text{-}H^+}(j1)$[c]	$\Delta(\Delta H_{ads\text{-}H^+})$[d] (kJ mol^{-1})	$\Delta(\Delta S_{ads\text{-}H^+})$[d] (J mol^{-1} K^{-1})
AEL	5.3	0.62	−50.9	−70.3	9.8	0.93	0.1	−0.5
AFO	5.6	0.77	−51.4	−67.8	7.4	0.92	0.2	−0.4
TON	5.7	0.81	−56.1	−73.2	6.9	1.04	0.0	0.3
MTT	5.7	0.87	−50.1	−67.7	8.7	0.95	0.2	−0.2
ATO	6.1	1.00	−53.6	−68.1	5.5	0.92	1.2	0.9
MRE	6.2	1.00	−54.0	−65.9	3.4	0.97	0.6	0.5
IFR	6.3	0.86	−45.1	−50.1	0.1	0.75	0.2	−2.1
MTW	6.3	0.93	−47.9	−59.4	4.5	0.90	0.5	−0.3
SFE	6.5	0.71	−41.5	−53.1	6.0	0.78	0.4	−1.6
MOR	6.5	0.93	−43.0	−55.0	5.9	0.75	0.5	−1.7
SSY	6.6	0.66	−41.0	−52.7	6.2	0.73	0.5	−2.0
CAN	6.6	1.00	−51.3	−59.5	1.1	0.95	0.6	0.4
VET	6.6	1.00	−48.0	−61.2	5.7	0.86	0.5	−0.7
STO	6.7	0.66	−44.4	−54.8	4.4	0.82	0.4	−1.2
OSI	6.9	0.87	−44.6	−55.7	4.9	0.80	0.3	−1.4
SFN	7.3	0.73	−37.2	−49.5	7.5	0.72	0.2	−2.5
ATS	7.3	0.87	−40.4	−49.7	4.4	0.75	0.3	−2.1
SFH	7.6	0.74	−37.1	−49.2	7.4	0.72	0.2	−2.6
AFI	8.1	1.00	−39.0	−48.4	4.8	0.67	0.4	−2.8
AET	8.2	0.91	−34.7	−51.7	11.6	0.69	0.2	−2.9
DON	8.7	0.99	−34.9	−47.9	8.6	0.72	0.1	−2.6
ETR	10.0	1.00	−29.7	−49.4	14.9	0.75	0.1	−2.3
VFI	12.0	1.00	−27.1	−46.0	14.9	0.72	−0.1	−2.8

[a]Pore-limiting diameter (PLD) and channel diameter ratio taken from Table 1. [b]Quantities correspond to Boltzmann averages over all bonds j and T-sites i as described in section 2. [c]Ratios of the equilibrium constant for adsorption through a central (j = 2) bond to that for a terminal bond (j = 1). [d]Differences in enthalpy and entropy for the formation of a central cracking reactant state versus a terminal cracking reactant state.

materials such as enzymes that are exploited for their shape-specificity,[49,50] and in adsorption is expected to be strongest for homologous series of materials that are structurally similar.[51] As discussed in section 3.2, by changing the topology more noticeably (e.g., introducing cages) rather than changing the channel dimensions, this compensation partly breaks down and $\Delta A_{ads\text{-}H^+}$ can be tuned with greater control.

Thus far, the discussion has been centered on the thermodynamics of adsorption for *n*-butane as a whole, Boltzmann-averaged over all three C−C bonds j (j = 1 for terminal bonds, j = 2 for the central bond). However, different sets of thermodynamic parameters can be calculated for each bond (see section 2). The ratio of the equilibrium constant for adsorption to form different C−C reactant states (j = 1, j = 2) determines the selectivity to adsorption of butane via different C−C bonds, which in turn affects the selectivity of monomolecular cracking reactions (in addition to intrinsic kinetics). Recent studies of the effects of the zeolite structure on the kinetics of these reactions can be found elsewhere.[34,52] An analysis of the dependence of the ratio of equilibrium constants for formation of different reactant states, and of the configurations that *n*-butane adopts in each of these adsorbed states, on zeolite structural parameters provides insight on the mechanisms by which structural parameters influence adsorption, as discussed below.

The ratio of the equilibrium constant for the adsorption of *n*-butane to form a reactant state for central cracking to that for forming a reactant state for terminal cracking at 773 K ($K_{ads\text{-}H^+}(j2)/K_{ads\text{-}H^+}(j1)$) was calculated using eq 1 and is plotted vs PLD in Figure 6. It can be seen that, as PLD increases, the selectivity to the formation of a reactant state for central cracking decreases until the PLD reaches ∼8 Å and then increases slightly for PLDs of 8−12 Å. Plots of the differences in enthalpy and entropy for formation of a central cracking reactant state vs a terminal cracking reactant state ($\Delta(\Delta H_{ads\text{-}H^+})$ and $\Delta(\Delta S_{ads\text{-}H^+})$) are shown in parts a and b of Figure 7, respectively. Both $\Delta(\Delta H_{ads\text{-}H^+})$ and $\Delta(\Delta S_{ads\text{-}H^+})$ generally decrease as PLD increases for zeolites with PLD > 6 Å (zeolites for which repulsive interactions were not inferred to be influencing thermodynamics). It can be seen that the changes in $K_{ads\text{-}H^+}(j2)/K_{ads\text{-}H^+}(j1)$ (Figure 6) with respect to PLD mirror the changes in $\Delta(\Delta S_{ads\text{-}H^+})$ (Figure 7b). The ratio of equilibrium constants is thus controlled primarily by $\Delta(\Delta S_{ads\text{-}H^+})$, and the negative values determined for this quantity show that *n*-butane experiences greater freedom of movement when adsorbed via a $j1$ vs a $j2$ bond, and that the $j1$ state benefits entropically from a decrease in confinement below a critical PLD, discussed below.

The influences of PLD and diameter ratio on $K_{ads\text{-}H^+}(j2)/K_{ads\text{-}H^+}(j1)$ seen in Figure 6 are consistent with the increased rotational movement of *n*-butane expected for an increase in pore size. As the PLD increases or as the diameter ratio decreases, *n*-butane has more room to rotate freely and should be more likely to orient perpendicular to rather than parallel to the channel wall in configurations that maximize the probability of $j1$ adsorption. The perpendicular configurations involve less contact with the channel walls relative to parallel orientations that promote less $j1$ adsorption and more $j2$ adsorption. Therefore, $\Delta(\Delta S_{ads\text{-}H^+})$ decreases, driving a corresponding decrease in $K_{ads\text{-}H^+}(j2)/K_{ads\text{-}H^+}(j1)$. As the PLD approaches the length of *n*-butane (∼8 Å),[23] the molecule can rotate relatively freely while contacting both sides of the channel, thereby reducing the loss in enthalpic stabilization[23,24] that would occur for an increase in PLD beyond

DOI: 10.1021/acs.jpcc.6b09703
J. Phys. Chem. C 2017, 121, 1618−1638

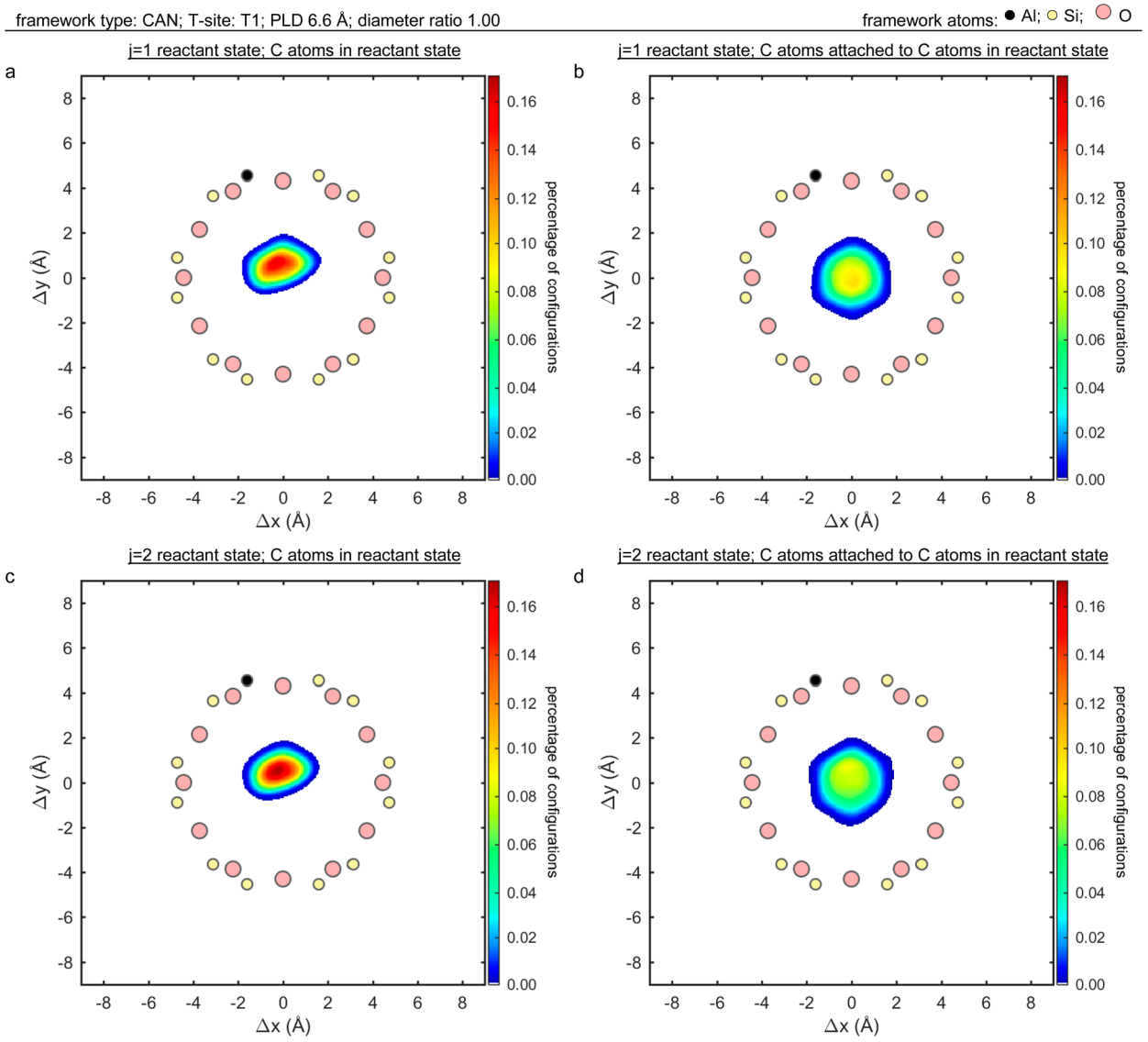

Figure 3. Heat maps that show the percentage of C atom coordinates that fall within square areas of side length 0.06 Å for configurations of *n*-butane adsorbed in a reactant state at site T1 in CAN, obtained using NVT simulations. The plane of view is perpendicular to the channel direction, and the origin corresponds to the channel center. Zeolite atoms located at the channel perimeter are indicated with circles.

this critical value. As the PLD increases further, the molecule can no longer rotate freely without losing contact with one side of the channel. With further increases in PLD, therefore, $K_{ads\text{-}H^+}(j2)/K_{ads\text{-}H^+}(j1)$ increases slightly and then plateaus.

Heat maps generated using NVT simulations that show the distribution of C atoms of *n*-butane in a reactant state as a function of PLD for CAN, AFI, and VFI confirm these interpretations. Heat maps viewed perpendicular to the channels are presented for CAN (PLD 6.6, diameter ratio 1.00), AFI (PLD 8.1 Å, diameter ratio 1.00), and VFI (PLD 12.0 Å, diameter ratio 1.00) in Figures 3, 8, and 9, respectively. (The views parallel to the channels are given in section S.4 of the Supporting Information.) Starting with CAN, which has the smallest PLD, it can be seen from the heat map in Figure 3 that the distribution of C atoms for the two atoms in the reactant state appears similar for both *j*1 and *j*2 adsorption, as do the distributions of the remaining two atoms. The maximum intensity for both types of reactant states (*j*1 and *j*2) and for reactant-state atoms vs the remaining atoms is located near the center of the channel (the same is observed for the view parallel to the channel; see Figure S.12). The similar distances of the maxima for reactant-state atoms and for the remaining atoms from the channel center axis indicate that butane orients parallel to the channel in CAN, consistent with the size of the PLD relative to *n*-butane (~4.3 × 8 Å), and with the conclusion discussed above that PLDs of 6−7 Å provide optimal enthalpic interactions with *n*-butane. The predominance of parallel orientations of *n*-butane in CAN is also consistent with the near equal preference for adsorption via a *j*1 vs *j*2 bond, reflected in the value of 0.95 determined for $K_{ads\text{-}H^+}(j2)/K_{ads\text{-}H^+}(j1)$.

Moving to AFI (Figure 8), which has a PLD of 8.1 Å, significant changes occur in the relative distributions of the two reactant-state atoms and the two attached atoms for *j*1 versus *j*2 adsorption. While for both *j*1 and *j*2 the C atoms in a reactant state are distributed similarly, the remaining C atoms explore a larger area for the *j*1 state than for the *j*2 state. The atoms that are attached to reactant-state C atoms for *j*1 adsorption are nearly centered within the channel, while the reactant-state C atoms are concentrated near the Al atom. By contrast to the case for *j*1, the atoms attached to the reactant-state C atoms for *j*2 adsorption

DOI: 10.1021/acs.jpcc.6b09703
J. Phys. Chem. C 2017, 121, 1618−1638

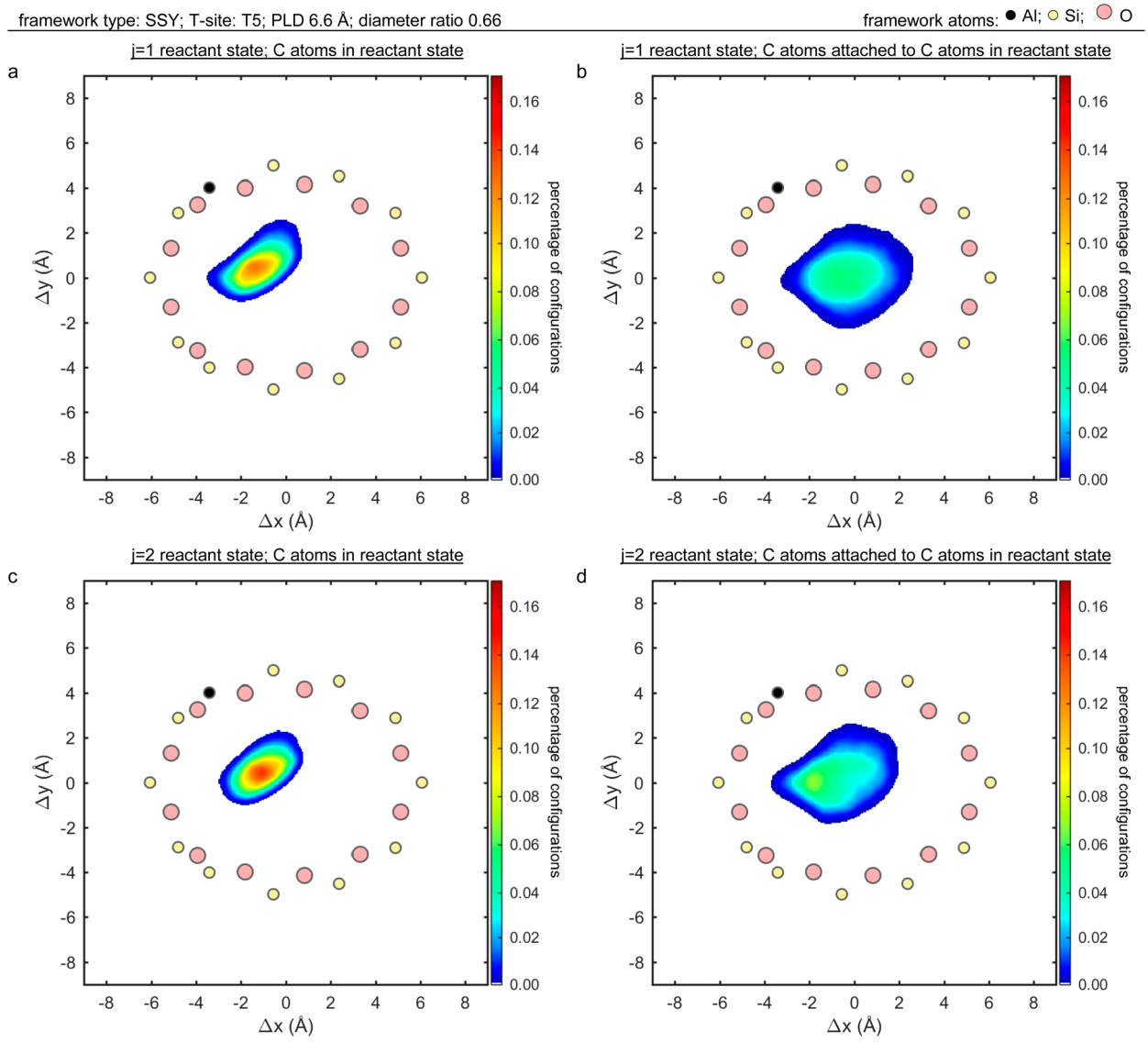

Figure 4. Heat maps that show the percentage of C atom coordinates that fall within square areas of side length 0.06 Å for configurations of *n*-butane adsorbed in a reactant state at site T5 in SSY, obtained using NVT simulations. The plane of view is perpendicular to the channel direction, and the origin corresponds to the channel center. Zeolite atoms located at the channel perimeter are indicated with circles.

are not centered within the channel, and their distribution is skewed toward the active site. These data support the conclusion that channels with PLDs similar to the length of an *n*-alkane promote configurations in which the molecule is not oriented parallel to the channel. These nonparallel orientations favor adsorption via a terminal bond and are associated with higher entropy. Consequently, the values of $K_{ads\text{-}H^+}(j2)/K_{ads\text{-}H^+}(j1)$ and $\Delta(\Delta S_{ads\text{-}H^+})$ are lower for AFI relative to CAN. As discussed below, as the PLD becomes larger and exceeds the length of *n*-butane (~8 Å), the interaction of *n*-butane with the channel wall opposite the active site becomes less significant, and these quantities lose their sensitivity to confinement.

Heat maps of the locations of C atoms of *n*-butane adsorbed at site T2 in VFI, viewed perpendicular to the channel, are presented in Figure 9. For both *j*1 and *j*2 adsorption and for the two reactant-state atoms as well as the two remaining atoms, the distributions are more diffuse and are in close proximity to fewer zeolite O atoms in VFI (PLD 12.0 Å) than in AFI (PLD 8.1 Å), consistent with the higher values of $\Delta S_{ads\text{-}H^+}$ and $\Delta H_{ads\text{-}H^+}$ determined for VFI. As for AFI, in VFI, the C atoms attached to the reactant-state C atoms for the *j*1 reactant state are located farther, on average, from the channel center than are those for the *j*2 state, consistent with the contribution of orientations in which *n*-butane is not parallel to the channels. However, for VFI, the C atoms are concentrated on one side of the channel due to its large diameter, and *n*-butane effectively does not "see" the channel wall opposite the Al atom. Therefore, even though *n*-butane may rotate relatively freely within VFI, the perpendicular orientations are slightly less preferred relative to AFI, causing $K_{ads\text{-}H^+}(j2)/K_{ads\text{-}H^+}(j1)$ to be higher for VFI. The observation that this ratio is lowest for AFI, therefore, can be attributed to subtle enthalpic benefits associated with the match in size between the pore diameter and the length of *n*-butane. On the basis of the above physical picture, the PLD at which the minimum in $K_{ads\text{-}H^+}(j2)/K_{ads\text{-}H^+}(j1)$ occurs is also expected to scale with the length of the *n*-alkane. As shown in the Supporting Information (Figure S.5), $K_{ads\text{-}H^+}(j2)/K_{ads\text{-}H^+}(j1)$ occurs at a larger PLD for *n*-pentane and *n*-hexane relative to *n*-butane.

3.2. Effects of Cages for Zeolites Having Circular Pores.

The influence of cages on *n*-butane adsorption is investigated

DOI: 10.1021/acs.jpcc.6b09703
J. Phys. Chem. C 2017, 121, 1618−1638

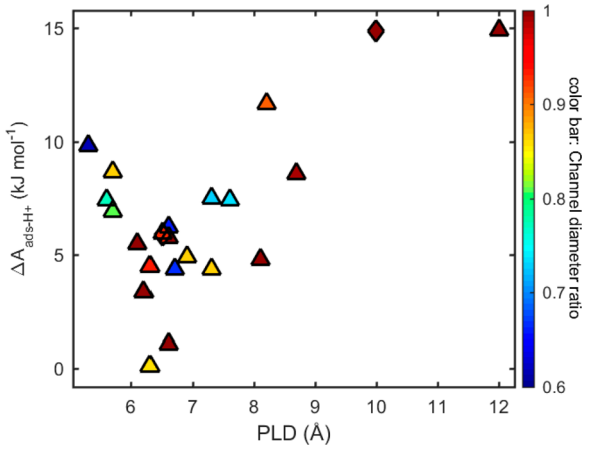

Figure 5. Helmholtz energy of adsorption at 773 K for *n*-butane adsorbed in a reactant state in one-dimensional zeolites vs the pore-limiting diameter (PLD). Diamonds correspond to zeolites with 8-MR side pockets and triangles to zeolites without side pockets. The color bar indicates the ratio of the minimum to maximum channel width given in Table 2.

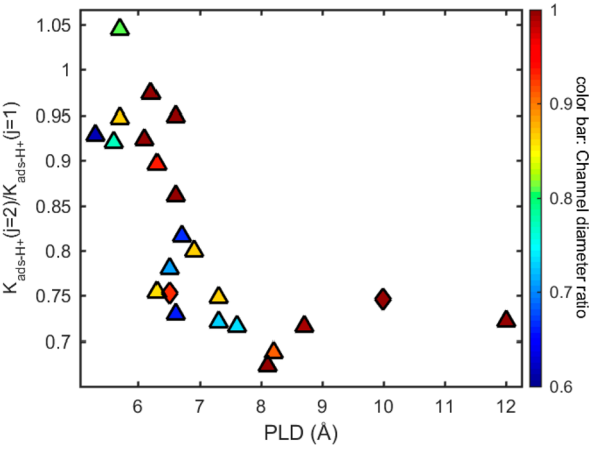

Figure 6. Ratio of the equilibrium constant for adsorption of *n*-butane via a central C−C bond ($j = 2$) to that for adsorption via a terminal C−C bond ($j = 1$) at 773 K for 1D zeolites without cages. Diamonds correspond to zeolites with 8-MR side pockets and triangles to zeolites without side pockets. The color bar indicates the ratio of the minimum to maximum channel width given in Table 2.

next. For the purpose of this analysis, only zeolites having a channel diameter ratio of 0.95−1.00 are considered, given the influence of this quantity on thermodynamics discussed in section 3.1. The zeolites analyzed in this section and their topological descriptors are given in Table 3 and the data for all plots in this section are included in Table 4. First, the effects of replacing channel space of a given PLD with cages of a larger diameter are discussed. The size of the cage is described using the largest cavity diameter (LCD),[48] the diameter of the largest sphere that can be contained within the cage. A simplified illustration of the topological differences between zeolites with and without cages and having the same PLD is given in Figure 10a. Next, zeolites with and without cages are compared at constant LCD, where the LCD and PLD are the same for zeolites that lack cages. The structural differences between zeolites with and without cages at fixed LCD are illustrated in Figure 10b.

Plots of $\Delta H_{ads\text{-}H^+}$ vs LCD and $\Delta S_{ads\text{-}H^+}$ vs LCD are presented in Figure 11. The effects of replacing channels with cages at fixed PLD can be observed by comparing triangular and circular data points of the same color. Two such sets of data can be seen on the plot. One set, represented with medium blue data points, corresponds to a PLD of ∼6.1 Å and a LCD of ∼8.3 Å, and includes two zeolites with cages (circles: SFF, STF) and two zeolites without cages (triangles: ATO, MRE). The second set is represented with green data points and includes AFI, which has only channels and a PLD of 8.1 Å, and LTL, which has a PLD of 8.1 Å and a LCD of 10.7 Å. It can be seen that, for the first set, replacing channels with cages (i.e., in moving from triangles to circles) increases both $\Delta H_{ads\text{-}H^+}$ and $\Delta S_{ads\text{-}H^+}$ as a result of the reduction in van der Waals contacts between the alkane and zeolite caused by the larger diameter of the cage. The significant increase in $\Delta S_{ads\text{-}H^+}$ (∼16 J mol^{-1} K^{-1}) is attributed primarily to a gain in rotational entropy, since the LCDs of SFF and STF (8.2 and 8.3 Å) are commensurate with the gas-phase gyration diameter of *n*-butane (7.67 Å).[23]

From the second set of data (shown by the green triangle and circle), it is evident that the increases in $\Delta S_{ads\text{-}H^+}$ and $\Delta H_{ads\text{-}H^+}$ upon introduction of cages 10.7 Å in diameter to channels 8.1 Å in diameter are very small compared to the changes in these parameters upon introducing ∼8.3 Å cages to 6.1 Å channels. In fact, $\Delta S_{ads\text{-}H^+}$ *decreases* by 2.7 J mol^{-1} K^{-1}, suggesting that *n*-butane has less freedom of movement within LTL than in AFI. This conclusion may appear to be counterintuitive, given the larger diameter of the cages of LTL compared to the channels of AFI. As discussed below, this result can be explained on the basis of the shape of the LTL cage, which is not well represented by a 10.7 Å sphere. Adjacent cages of LTL intersect to form a pocket[53] 2.8 Å deep and 5.3 Å wide that encircles the channel. This geometry can be seen in heat maps of the C atom distributions of *n*-butane in a reactant state, viewed parallel to the channels, presented in Figure 12 (the view perpendicular to the channels is provided in the Supporting Information, Figure S.16).

It can be seen from Figure 12 (and Figure S.16) that the pockets formed by the LTL cages partially contain *n*-butane (∼4.3 × 8.3 Å)[54] with its long dimension oriented toward the channel center. This orientation can be inferred on the basis of the proximity of the maximum in the distribution of C atoms attached to reactant-state C atoms to the cage center. The maximum for this distribution is located closer to the cage center than is the maximum in the distribution of reactant-state C atoms. The dimensions of this pocket are much smaller than those of the 10.7 Å sphere used to describe the LCD; as a result, the pocket appears to provide more enthalpic stabilization to *n*-butane than expected for such a sphere.[47,55] In addition, the 5.3 Å width of the pocket, which is smaller than the long dimension of *n*-butane (∼8 Å), prevents free rotation of *n*-butane about an axis orthogonal to the channel, a conclusion that is consistent with the more diffuse distribution for C atoms viewed perpendicular to (Figure S.16) vs parallel to (Figure 12) the channels. Consequently, the changes in $\Delta H_{ads\text{-}H^+}$ and $\Delta S_{ads\text{-}H^+}$ in moving from the 8.1 Å channels of AFI to the 10.7 Å cages of LTL are small relative to the changes that would be expected if the cages of LTL truly resembled 10.7 Å spheres. This conclusion provides motivation for identifying topological descriptors that define the dimensions of cages based on their actual shapes rather than on a convenient, preselected shape.

By contrast to the effects of introducing cages larger in diameter than the channels, the effects of replacing channels of a given diameter with cages of the same diameter (Figure 10b) increases the attractive van der Waals interactions between the alkane and zeolite,[47,55] provided the alkane can fully fit within the

DOI: 10.1021/acs.jpcc.6b09703
J. Phys. Chem. C 2017, 121, 1618−1638

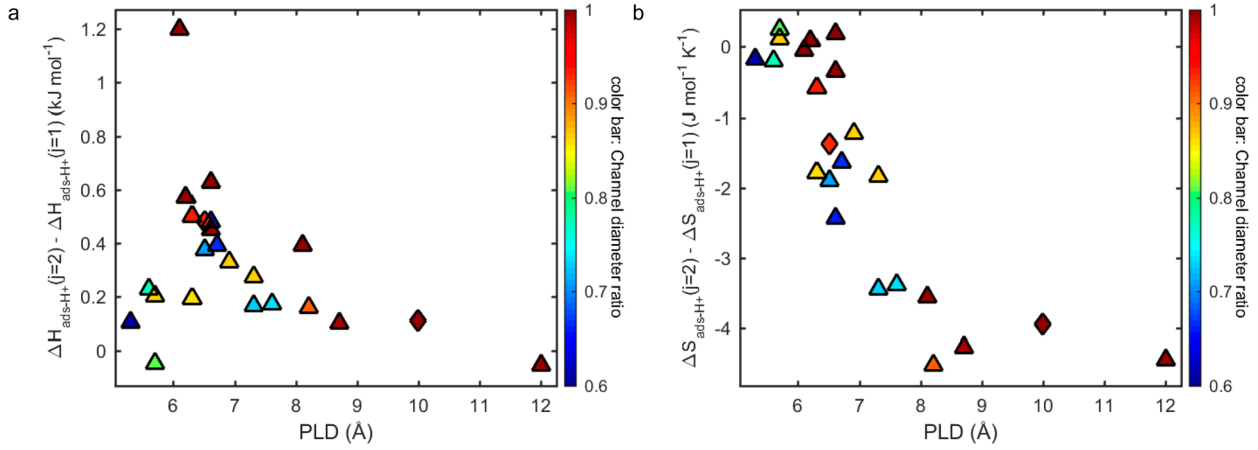

Figure 7. Difference in (a) enthalpy and (b) entropy of adsorption for *n*-butane adsorbed via a central C−C bond ($j = 2$) vs a terminal C−C bond ($j = 1$) at 773 K for 1D zeolites without cages. Diamonds correspond to zeolites with 8-MR side pockets and triangles to zeolites without side pockets. The color bar indicates the ratio of the minimum to maximum channel width given in Table 2.

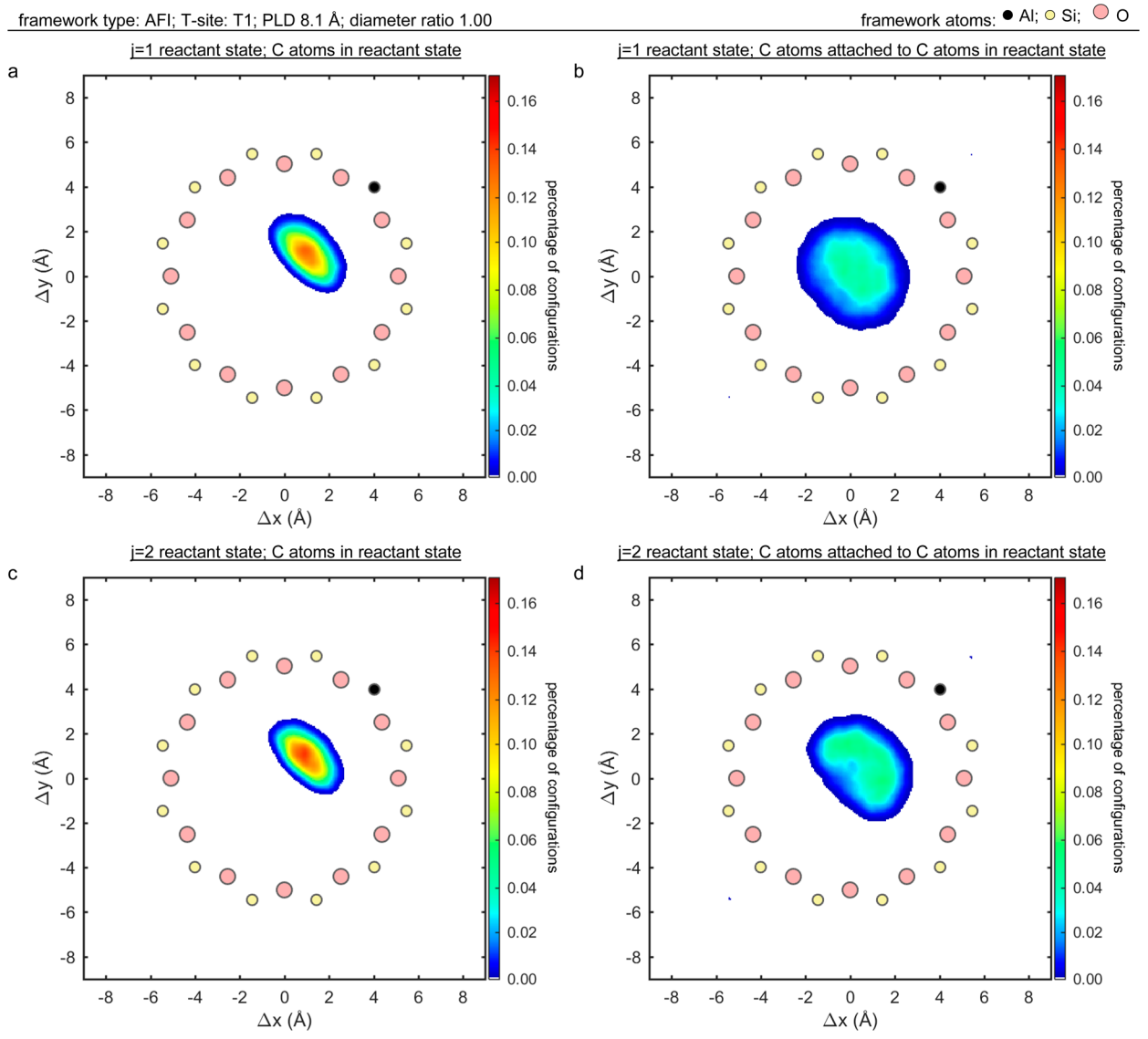

Figure 8. Heat maps that show the percentage of C atom coordinates that fall within square areas of side length 0.06 Å for configurations of *n*-butane adsorbed in a reactant state at site T1 in AFI, obtained using NVT simulations. The plane of view is perpendicular to the channel direction, and the origin corresponds to the channel center. Zeolite atoms located at the channel perimeter are indicated with circles.

DOI: 10.1021/acs.jpcc.6b09703
J. Phys. Chem. C 2017, 121, 1618−1638

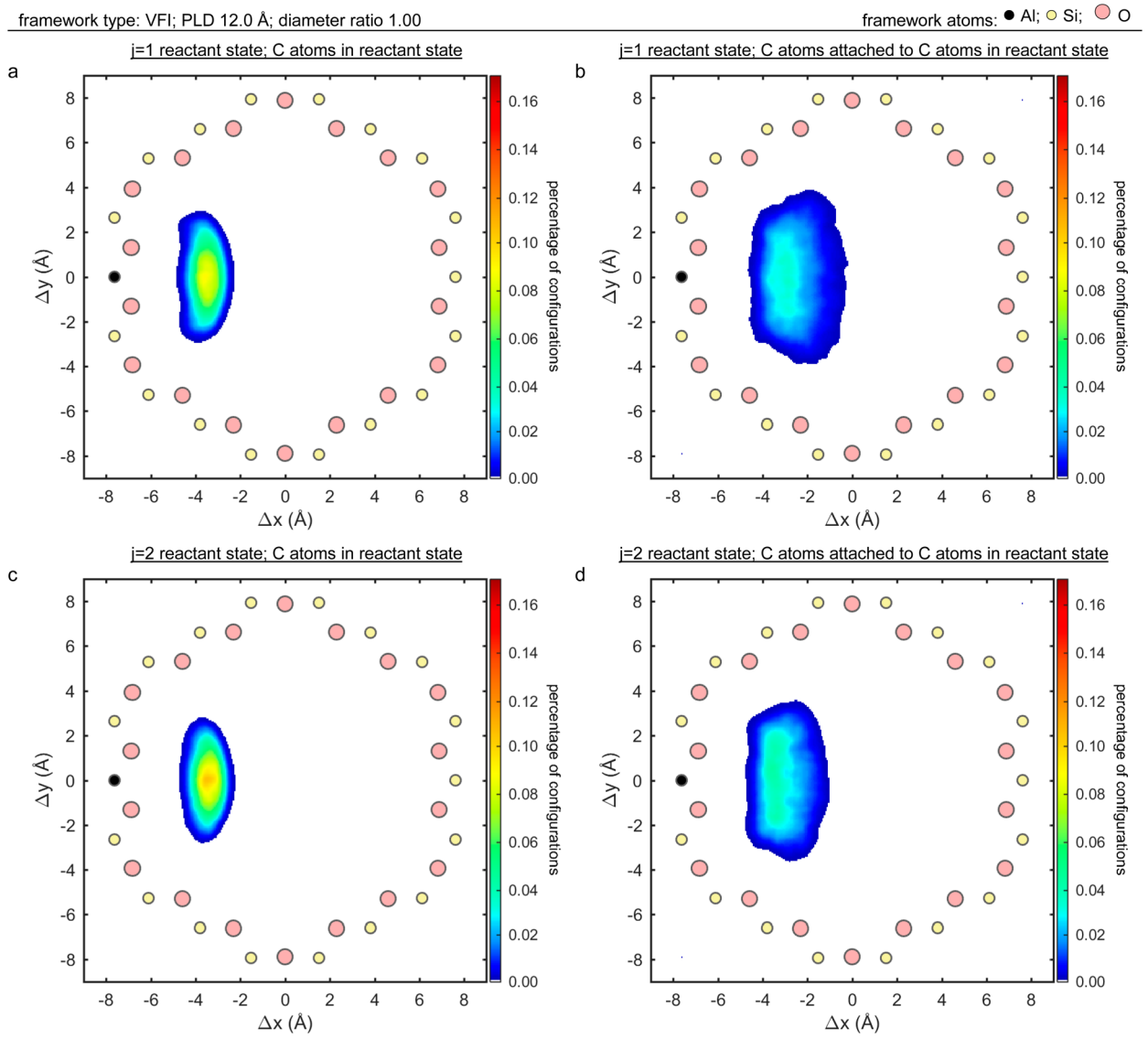

Figure 9. Heat maps that show the percentage of C atom coordinates that fall within square areas of side length 0.06 Å for configurations of *n*-butane adsorbed in a reactant state at site T2 in VFI, obtained using NVT simulations. The plane of view is perpendicular to the channel direction, and the origin corresponds to the channel center. Zeolite atoms located at the channel perimeter are indicated with circles.

cage. Figure 11a shows that $\Delta H_{ads\text{-}H^+}$ is more negative for zeolites with cages than for zeolites without cages when the LCD is at least equal to the length of *n*-butane (~8 Å). By contrast, for BOF, which has a LCD of only 6.2 Å, $\Delta H_{ads\text{-}H^+}$ is higher relative to zeolites that have only channels of diameter ~6.2 Å. On the basis of the discussion in section 3.1, this observation can be attributed to the contributions of repulsive interactions, since the channel diameter of BOF is less than 4.7 Å (based on IZA tabulated data) and *n*-butane cannot fit fully within the 6.2 Å cage.[13,14,25] The decrease in $\Delta H_{ads\text{-}H^+}$ that occurs upon introduction of cages having diameters larger than 8 Å does not appear to be caused by deviations of the actual cage geometry from spherical, as was observed for LTL, since Figure 11b shows that $\Delta S_{ads\text{-}H^+}$ is not commensurately lower for zeolites with cages than for zeolites with channels. In addition, the decrease in $\Delta H_{ads\text{-}H^+}$ is larger when moving from AFI (PLD and LCD of 8.1 Å) to AWW (LCD 8.1 Å, PLD 4.8 Å) than when moving from AFI to SFF or STF (LCD ~ 8.2 Å, PLD ~ 5.9 Å), which have nearly the same LCD but a larger PLD than AWW. This behavior is consistent with the greater surface area of a cage having smaller channel openings.

The importance of the match in size between *n*-butane and the cage is also apparent from the changes in $\Delta S_{ads\text{-}H^+}$ upon the introduction of cages. Figure 11b shows that, for LCDs of 8−10 Å, $\Delta S_{ads\text{-}H^+}$ is similar for zeolites with and without cages. The similarity of $\Delta S_{ads\text{-}H^+}$ at fixed LCD for channels and cages suggests that *n*-butane experiences similar freedom of movement in both environments. Configurational data for *n*-butane adsorbed at site T3 in STF, presented in Figure 13 (viewed perpendicular to the channel) and in Figure 14 (viewed parallel to the channel), are consistent with this picture. (Small and thermodynamically insignificant portions of the distributions for the *j*1 reactant-state atoms that appear outside of the STF cage result because the Al atom is marginally accessible from an adjacent cage.) By comparing Figure 8, which shows the configurational data for AFI (PLD and LCD 8.1 Å), to Figures 13 and 14, which show the configurations for STF (PLD 6.0 Å, LCD 8.3 Å), it can be seen that *n*-butane orients perpendicular to the channel to some extent in both zeolites and is nearly centered within the channel or cage. The molecule also explores a similar amount of pore space in each zeolite, consistent with the similar values

DOI: 10.1021/acs.jpcc.6b09703
J. Phys. Chem. C 2017, 121, 1618−1638

Table 3. IZA Framework Types and Material Names (in Parentheses), Pore-Limiting Diameter (PLD), Channel Diameters and Ratio of Channel Diameters, Largest Cavity Diameter (LCD), and Percentage of Pore Volume in the Cages

	channel properties				cage properties	
framework type and material name	ring size (T atoms)	PLD[b] (Å)	diameter[c] (Å)	diameter ratio[c] (Å)	LCD[b] (Å)	percentage of pore volume[b]
AFI (AlPO-5)	12	8.1	7.3 × 7.3	1.00	8.1	0
ATO (AlPO-31)	12	6.1	5.4 × 5.4	1.00	6.1	0
AWW (AlPO-22)	8	4.8	3.9 × 3.9	1.00	8.1	78
BOF (UCSB-15GaGe)	10	4.3	5.2 × 5.4	0.96	6.2	86
CAN (Cancrinite)	12	6.6	5.9 × 5.9	1.00	6.6	0
DON (UTD-1F)	14	8.7	8.1 × 8.2	0.99	8.7	0
ETR (ECR-34)	18[a]	10.0	10.1 × 10.1	1.00	10.0	0
LTL (Linde type L)	12	8.1	7.1 × 7.1	1.00	10.7	47
MRE (ZSM-48)	10	6.2	5.6 × 5.6	1.00	6.2	0
SAS (STA-6)	8	4.9	4.2 × 4.2	1.00	9.6	77
SFF (SSZ-44)	10	5.9	5.4 × 5.7	0.95	8.2	77
STF (SSZ-35)	10	6.0	5.4 × 5.7	0.95	8.3	85
VET (VPI-8)	12	6.6	5.9 × 5.9	1.00	6.6	0
VFI (VPI-5)	18	12.0	12.7 × 12.7	1.00	12.0	0

[a]ETR also contains 8-MR side pockets ∼2.5 Å along the shorter dimension that are essentially inaccessible at 773 K.[30] [b]Pore-limiting diameter (PLD), largest cavity diameter (LCD), and percentage of pore volume in accessible cages calculated by First et al.[48] [c]Channel diameters taken from the IZA database, and ratio of minimum to maximum diameter.

Table 4. Thermodynamic Quantities Obtained Using CBMC Simulations for Adsorption of *n*-Butane at 773 K in One-Dimensional Zeolites having Circular Channels, Listed in Order of Increasing LCD

framework type	LCD[a] (Å)	PLD[a] (Å)	$\Delta H_{ads\text{-}H^+}$[b] (kJ mol^{-1})	$\Delta S_{ads\text{-}H^+}$[b] (J mol^{-1} K^{-1})	$\Delta A_{ads\text{-}H^+}$[b] (kJ mol^{-1})	$K_{ads\text{-}H+}(j2)/K_{ads\text{-}H+}(j1)$[c]	$\Delta(\Delta H_{ads\text{-}H^+})$[d] (kJ mol^{-1})	$\Delta(\Delta S_{ads\text{-}H^+})$[d] (J mol^{-1} K^{-1})
ATO	6.1	6.1	−53.6	−68.1	5.5	0.92	1.2	0.9
BOF	6.2	4.3	−49.8	−73.0	13.1	1.06	−0.4	0.0
MRE	6.2	6.2	−54.0	−65.9	3.4	0.97	0.6	0.5
CAN	6.6	6.6	−51.3	−59.5	1.1	0.95	0.6	0.4
VET	6.6	6.6	−48.0	−61.2	5.7	0.86	0.5	−0.7
AWW	8.1	4.8	−51.2	−55.3	−2.1	0.64	0.1	−3.6
AFI	8.1	8.1	−39.0	−48.4	4.8	0.67	0.4	−2.8
SFF	8.2	5.9	−46.2	−52.2	0.6	0.68	0.4	−2.6
STF	8.3	6.0	−46.0	−50.4	−0.6	0.68	0.4	−2.8
DON	8.7	8.7	−34.9	−47.9	8.6	0.72	0.1	−2.6
SAS	9.6	4.9	−41.7	−45.9	0.2	0.66	0.3	−3.1
ETR	10.0	10.0	−29.7	−49.4	14.9	0.75	0.1	−2.3
LTL	10.7	8.1	−38.1	−51.1	7.8	0.77	−0.4	−2.7
VFI	12.0	12.0	−27.1	−46.0	14.9	0.72	−0.1	−2.8

[a]Pore-limiting diameter (PLD) and largest cavity diameter (LCD) taken from Table 3. [b]Quantities correspond to Boltzmann averages over all bonds j and T-sites i as described in section 2. [c]Ratios of equilibrium constant for adsorption through a central (j = 2) bond to that for a terminal bond (j = 1). [d]Differences in enthalpy and entropy for the formation of a central cracking reactant state versus a terminal cracking reactant state.

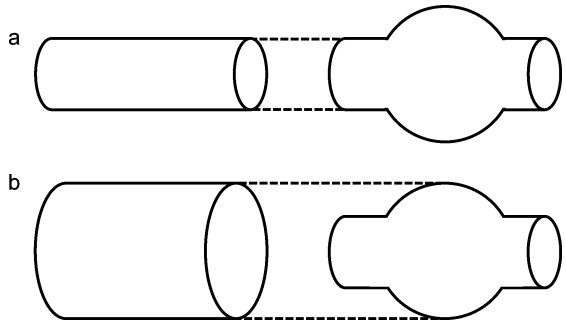

Figure 10. Representations of the pore topology of one-dimensional zeolites with (left) and without (right) cages and having (a) the same PLD or (b) the same LCD. In part a, the dashed lines connect channels of equal size in different zeolites, and in part b, the dashed lines connect a channel in one zeolite having the same diameter as a cage in another zeolite.

determined for $\Delta S_{ads\text{-}H^+}$. However, the distribution of *n*-butane in STF, especially for the *j*1 state, closely fits the contours of the cage and thus the molecule interacts with a larger surface area of the zeolite than when adsorbed in AFI, leading to a lower value of $\Delta H_{ads\text{-}H^+}$ for STF, as noted above. By contrast, when *n*-butane cannot fully fit within the cage, as is the case for BOF (LCD 6.2 Å), movement is more hindered relative to zeolites that have only channels of the same diameter (ATO, MRE),[23] and $\Delta S_{ads\text{-}H^+}$ is correspondingly more negative.

These interpretations of the effects of the match in size between the alkane and the cages are also supported by results for *n*-pentane and *n*-hexane, presented in the Supporting Information (Figure S.8). By contrast to *n*-butane, a much larger decrease in $\Delta S_{ads\text{-}H^+}$ occurs for these longer alkanes upon replacing channels of diameter ∼8 Å with cages of the same diameter. This result can be attributed to the inability of *n*-pentane and *n*-hexane to fit completely within cages of ∼8 Å and to, therefore, move

DOI: 10.1021/acs.jpcc.6b09703
J. Phys. Chem. C 2017, 121, 1618−1638

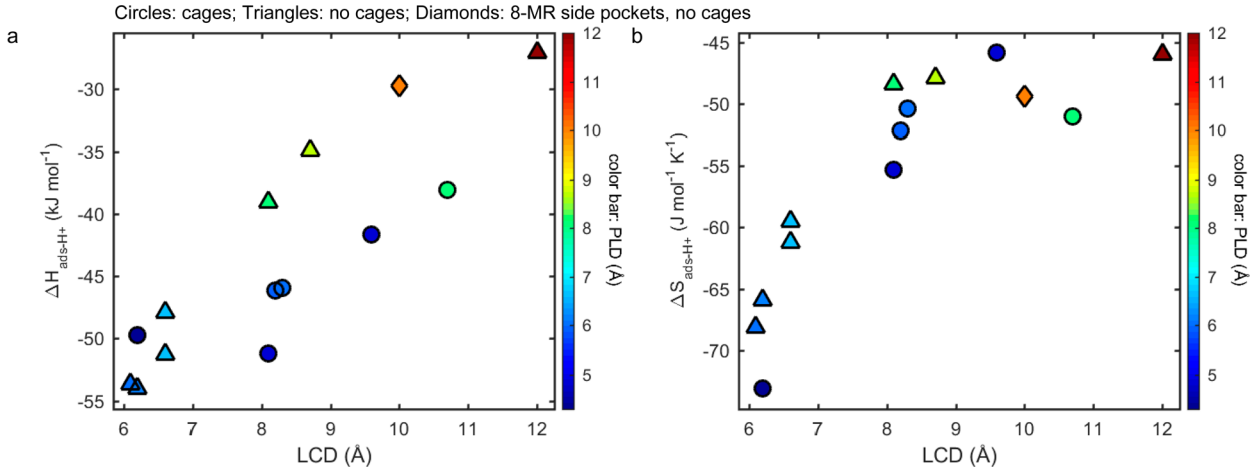

Figure 11. (a) Enthalpy of adsorption and (b) entropy of adsorption at 773 K for *n*-butane adsorbed in a reactant state in one-dimensional zeolites vs the largest cavity diameter (LCD). The color bar indicates the pore-limiting diameter (PLD) given in Table 4.

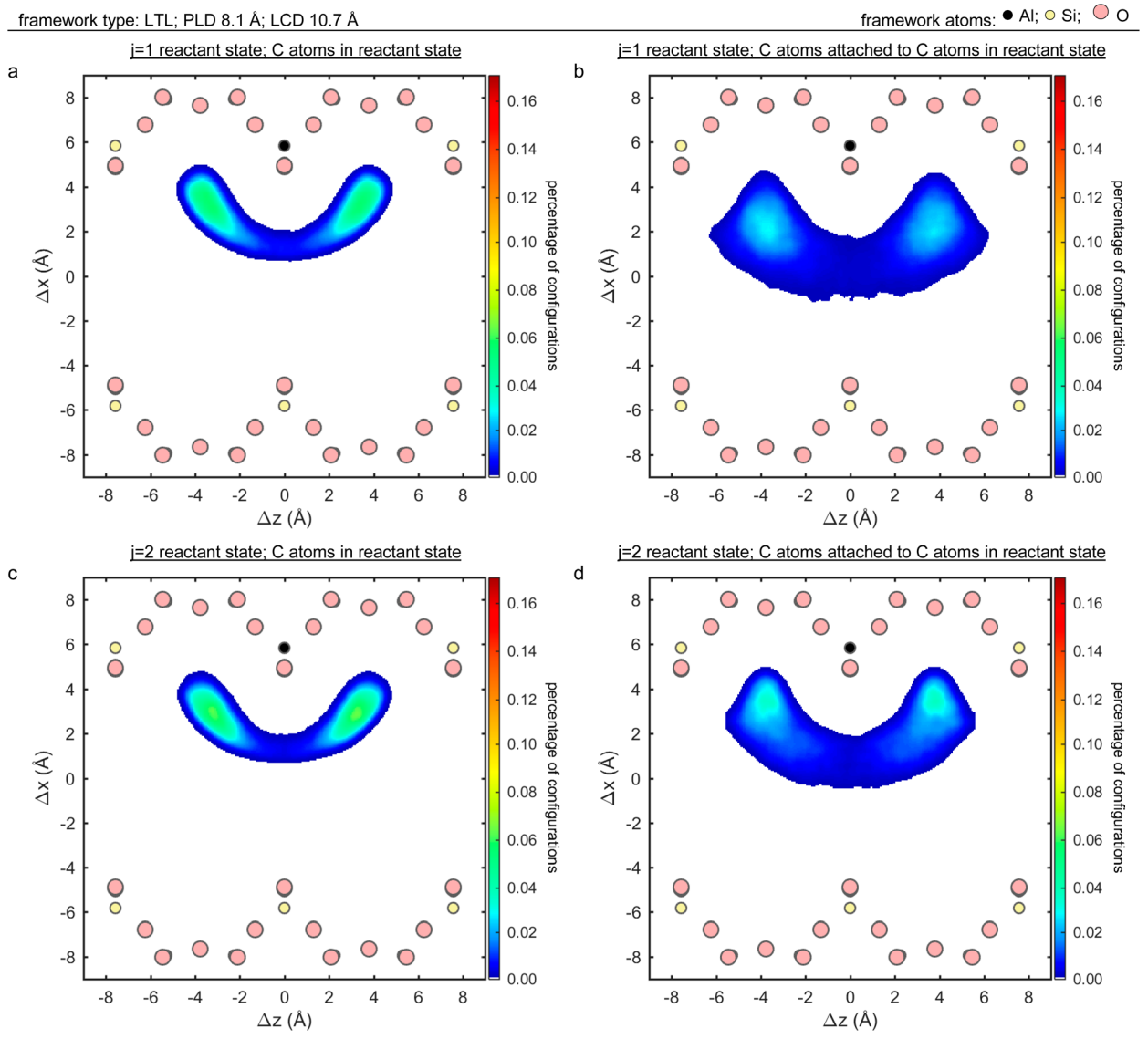

Figure 12. Heat maps that show the percentage of C atom coordinates that fall within square areas of side length 0.06 Å for configurations of *n*-butane adsorbed in a reactant state at site T2 in LTL, obtained using NVT simulations. The plane of view is parallel to the channel center axis and has been rotated in order to contain the Al atom. The origin corresponds to the channel center and the horizontal location of the Al atom. Zeolite atoms are located at the perimeter of the channel, and cages are indicated with circles.

DOI: 10.1021/acs.jpcc.6b09703
J. Phys. Chem. C 2017, 121, 1618−1638

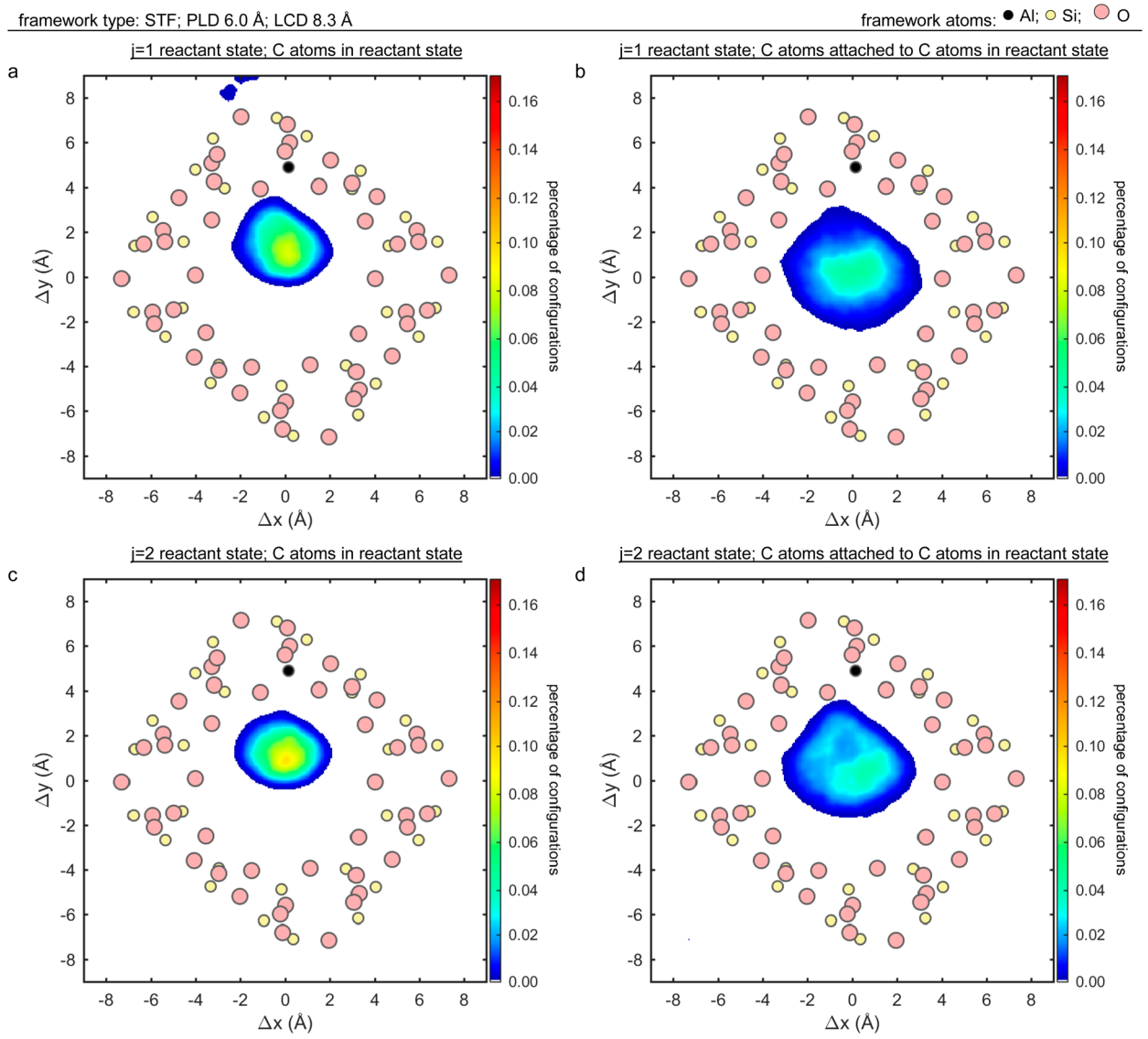

Figure 13. Heat maps that show the percentage of C atom coordinates that fall within square areas of side length 0.06 Å for configurations of *n*-butane adsorbed in a reactant state at site T3 in STF, obtained using NVT simulations. The plane of view is perpendicular to the channel direction, and the origin corresponds to the channel center. Zeolite atoms located at and between the perimeters of the channel and cage are indicated with circles.

unhindered within the cages. In addition, Figure S.8 shows that, relative to *n*-butane, *n*-pentane experiences a lower degree of enthalpic stabilization and *n*-hexane experiences repulsion in moving from channels of diameter ~8 Å (AFI) to cages of diameter ~8 Å within AWW, which has a PLD of 4.8 Å. A repulsive effect on $\Delta H_{ads\text{-}H^+}$ of cages that are too small to contain the alkane is *not* observed for SFF and STF, which also have LCDs of ~8 Å but have PLDs of ~6 Å. This observation supports previous conclusions[14] that channels less than 4.7 Å in diameter lead to repulsive interactions (the channel diameter of AWW is 3.9 Å based on IZA tabulated data; see Table 3), and provides direction for tuning the zeolite structure in order to selectively adsorb alkanes on the basis of their size.

The effects on $\Delta H_{ads\text{-}H^+}$ and $\Delta S_{ads\text{-}H^+}$ of a change in topology from cages to channels for a given alkane are also analogous to those reported by Denayer et al.[23,24] for the effects of branching on the adsorption of alkane isomers within a given zeolite. These authors observed that the entropies of adsorption for *n*-butane and isobutane adsorbed within MWW are similar, while the enthalpy of adsorption is more negative for isobutane. The authors attributed the lower enthalpy for isobutane to a close match in size between the branched isomer and the MWW cage. Isobutane can, therefore, rotate freely within the cage while also maximizing its enthalpic interactions with the zeolite. By contrast, *n*-butane can only rotate freely within the intersection of the cage and channels, resulting in a similar entropy to isobutane but higher enthalpy because of lower van der Waals contacts within the intersection. Although adsorption specific to cages could not be proven, the conclusions of Denayer et al. are qualitatively in agreement with the above observations of the effects of a change in geometry from channels to cages at fixed diameter.

It has thus far been demonstrated that $\Delta H_{ads\text{-}H^+}$ for *n*-butane is lower for adsorption in cages relative to channels of the same diameter, while $\Delta S_{ads\text{-}H^+}$ is similar for both environments provided that the LCD exceeds the length of *n*-butane. As a result, the usual compensation between $\Delta H_{ads\text{-}H^+}$ and $\Delta S_{ads\text{-}H^+}$ breaks down when the pore geometry is changed at a fixed characteristic dimension, and differences in free energy result when channels are replaced with cages. A plot of $\Delta A_{ads\text{-}H^+}$ vs LCD

DOI: 10.1021/acs.jpcc.6b09703
J. Phys. Chem. C 2017, 121, 1618−1638

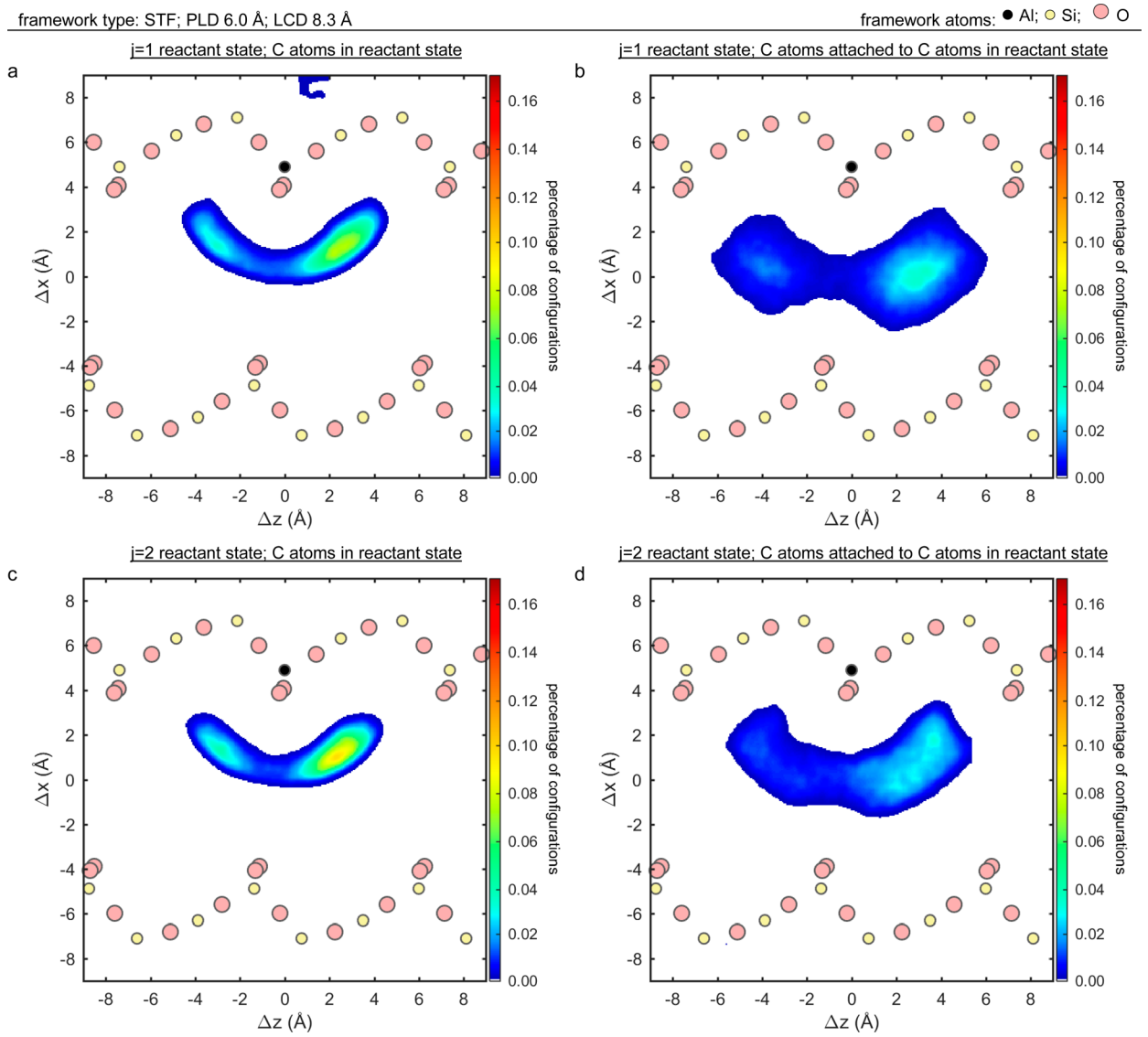

Figure 14. Heat maps that show the percentage of C atom coordinates that fall within square areas of side length 0.06 Å for configurations of *n*-butane adsorbed in a reactant state at site T3 in STF, obtained using NVT simulations. The plane of view is parallel to the channel center axis, and has been rotated in order to contain the Al atom. The origin corresponds to the channel center and the horizontal location of the Al atom. Zeolite atoms are located at the perimeter of the channel, and cages are indicated with circles.

is shown in Figure 15. It can be seen that, for LCDs exceeding 8 Å, $\Delta A_{ads\text{-}H^+}$ is lower for zeolites with cages than for zeolites without cages at fixed diameter because of the greater enthalpic stabilization provided by the cages. The value of $\Delta A_{ads\text{-}H^+}$ is minimized near a LCD of ∼8 Å because a cage of this size is large enough to allow free movement of *n*-butane, and, thus, a relatively high value for $\Delta S_{ads\text{-}H^+}$, but small enough to promote van der Waals contacts between the alkane and most of the cage surface. For larger LCDs, $\Delta A_{ads\text{-}H^+}$ increases because these van der Waals contacts are reduced without a significant gain in freedom of movement, while, for smaller LCDs (e.g., BOF), the repulsive interactions that result from the narrow PLD (4.3 Å) and from the small size of the LCD (6.2 Å) relative to *n*-butane increase $\Delta H_{ads\text{-}H^+}$ and decrease $\Delta S_{ads\text{-}H^+}$ relative to zeolites having the same LCD but only channels. Consequently, $\Delta A_{ads\text{-}H^+}$ for BOF is higher relative to ATO and MRE, which have channels of diameter ∼6 Å, for both enthalpic and entropic reasons. For zeolites for which repulsive forces do not contribute significantly to $\Delta H_{ads\text{-}H^+}$, however, enthalpy generally determines the relative values of $\Delta A_{ads\text{-}H^+}$ for adsorption in channels vs cages of the same diameter.

By contrast, upon introducing cages to channels at fixed PLD, both $\Delta H_{ads\text{-}H^+}$ and $\Delta S_{ads\text{-}H^+}$ increase and, as noted above, $\Delta A_{ads\text{-}H^+}$ decreases because the increase in $\Delta S_{ads\text{-}H^+}$ as a result of the decrease in confinement more than offsets the loss in enthalpic stabilization. This effect can be seen by comparing data indicated with medium blue triangles vs medium blue circles in Figure 15. The free energy change for such a change in geometry is, therefore, dominated by the increase in $\Delta S_{ads\text{-}H^+}$. However, the relative importance of $\Delta H_{ads\text{-}H^+}$ and $\Delta S_{ads\text{-}H^+}$ to $\Delta A_{ads\text{-}H^+}$ is expected to also depend on whether repulsive interactions are present, and such interactions were not inferred to exist for the sets of zeolites in this work that possess the same PLD but that have or do not have cages. The effects of changes in topology on $\Delta A_{ads\text{-}H^+}$ discussed above show that $\Delta A_{ads\text{-}H^+}$ can be systematically manipulated by changing from channels to cages at a fixed PLD or fixed LCD, although at 773 K this change is not in general dominated by either enthalpy or entropy. An advantage of

DOI: 10.1021/acs.jpcc.6b09703
J. Phys. Chem. C 2017, 121, 1618−1638

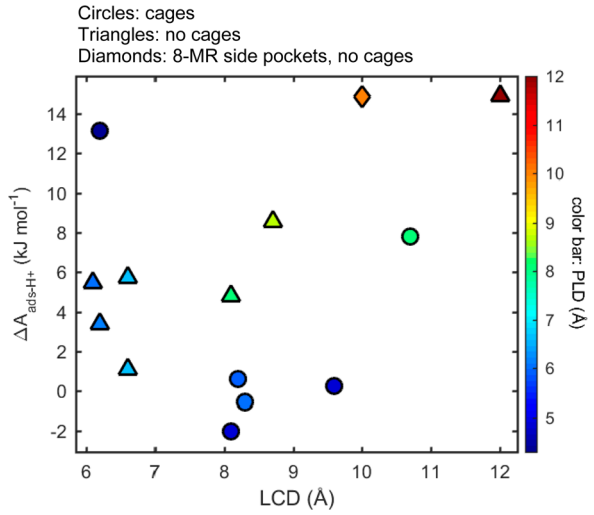

Figure 15. Helmholtz energy of adsorption at 773 K for *n*-butane adsorbed in a reactant state in one-dimensional zeolites vs the largest cavity diameter (LCD). The color bar indicates the pore-limiting diameter (PLD) given in Table 4.

manipulating $\Delta A_{ads\text{-}H^+}$ by introducing cages to straight channels at fixed LCD is that entropy−enthalpy compensation is largely circumvented when the cage diameter matches the gyration diameter of the alkane, enabling $\Delta H_{ads\text{-}H^+}$ to be controlled without significantly changing $\Delta S_{ads\text{-}H^+}$.

The last thermodynamic quantity to address is the ratio of the equilibrium constant for adsorption of *n*-butane via a central (j = 2) C−C bond to that for adsorption via a terminal (j = 1) C−C bond, $K_{ads\text{-}H^+}(j2)/K_{ads\text{-}H^+}(j1)$. A plot of this ratio vs LCD at 773 K is shown in Figure 17. Plots of the differences in $\Delta H_{ads\text{-}H^+}$ and in

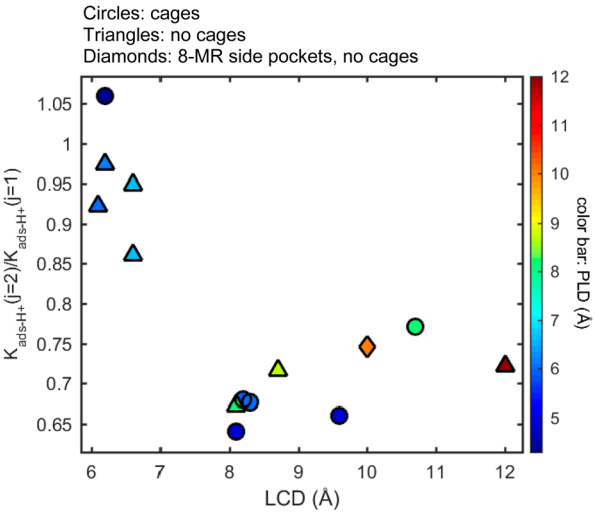

Figure 16. Ratio of the equilibrium constant for adsorption of *n*-butane via a central C−C bond (j = 2) to that for adsorption via a terminal C−C bond (j = 1) at 773 K for 1D zeolites with and without cages. The color bar indicates the pore-limiting diameter (PLD) given in Table 4.

$\Delta S_{ads\text{-}H^+}$ between $j2$ and $j1$ adsorption ($\Delta(\Delta H_{ads\text{-}H^+})$ and $\Delta(\Delta S_{ads\text{-}H^+})$) vs LCD are presented in Figure 15. As was observed for zeolites having only channels in section 3.1, the differences in $K_{ads\text{-}H^+}(j2)/K_{ads\text{-}H^+}(j1)$ for zeolites with cages are in general dominated by the value of $\Delta(\Delta S_{ads\text{-}H^+})$ and, therefore, by the relative freedom of movement of *n*-butane adsorbed via a central or terminal bond. Figure 16 shows that changes in $K_{ads\text{-}H^+}(j2)/K_{ads\text{-}H^+}(j1)$ with LCD for zeolites with cages follow qualitatively the same pattern as the data for zeolites with channels; the ratio initially decreases with increasing LCD and then increases again for larger LCDs. The same arguments that were used to rationalize the dependence of $K_{ads\text{-}H^+}(j2)/K_{ads\text{-}H^+}(j1)$ on PLD in section 3.1 also apply in the present context.

At the lowest LCD, an increase in LCD decreases confinement and increases the tendency of *n*-butane to orient perpendicular to the cage wall where it can adsorb in $j1$ reactant states. Because *n*-butane interacts less closely with the zeolite and can explore more pore space when in such orientations, its entropy is higher relative to the $j2$ reactant state. Therefore, $\Delta(\Delta S_{ads\text{-}H^+})$ also initially decreases as LCD increases. As the LCD continues to increase and becomes longer than a *n*-butane molecule (∼8 Å), the molecule continues to orient perpendicular to the cage wall but loses contact and, therefore, loses van der Waals interactions, with the opposite side of the cage. This conclusion is evident from the heat maps presented in Figures 13 and 14 for STF (LCD 8.3 Å) and in Figure 12 for LTL (LCD 10.7 Å). Thus, as the cage diameter increases beyond ∼8 Å, perpendicular orientations of the molecule and the associated $j1$ reactant states become less favored and $K_{ads\text{-}H^+}(j2)/K_{ads\text{-}H^+}(j1)$ increases again initially and appears to lose its sensitivity to confinement with further increases in LCD. This picture is consistent with the dependence of this ratio on LCD for longer alkanes; the upturn in $K_{ads\text{-}H^+}(j2)/K_{ads\text{-}H^+}(j1)$ for *n*-pentane and for *n*-hexane (shown in the Supporting Information, Figure S.10) appears to occur at a larger LCD than that for *n*-butane, consistent with the larger lengths of the former alkanes.

One notable difference in the appearance of the data sets for zeolites with and without cages is the apparently larger LCD at which the upturn in $K_{ads\text{-}H^+}(j2)/K_{ads\text{-}H^+}(j1)$ occurs when the LCD corresponds to a cage vs a channel. This result may originate in part from the greater surface area of cages relative to channels at the same diameter, which causes greater enthalpic stabilization of a freely rotating *n*-alkane molecule at fixed diameter. When the diameter of the cage is commensurate with the alkane length, perpendicular orientations and $j1$ reactant states may be preferred enthalpically because more of the cage surface contacts the alkane. Consistent with this proposal, the values of $\Delta(\Delta H_{ads\text{-}H^+})$ for *n*-pentane and *n*-hexane for an LCD of ∼9.5 Å (see Figure S.11) are higher when cages are present at fixed LCD. These results suggest that configurations in which an *n*-alkane spans the diameter of the cage or channel are preferred to a greater degree in cages vs in channels when the pore diameter is similar to the length of the alkane. Therefore, $K_{ads\text{-}H^+}(j2)/K_{ads\text{-}H^+}(j1)$ should generally be lower for zeolites with cages for LCDs of this size, as is observed in Figure 16 for *n*-butane and in Figure S.10 for *n*-pentane and *n*-hexane.

3.3. Screening of Zeolites Based on Free Energy of Adsorption and Reactant-State Selectivity. Using the relationships established between alkane adsorption thermodynamics and zeolite topology in sections 3.1 and 3.2, zeolites can be screened to assess what structural parameters to target in order to enhance the rate and selectivity of a catalytic reaction. As an example, the monomolecular cracking of *n*-butane at a central C−C bond is considered. Monomolecular cracking and dehydrogenation of a given alkane over a given zeolite occur at comparable rates (within a factor of 15; see ref 34, Table S.7) at Brønsted-acid sites in the limit of zero conversion. The intrinsic reaction is rate-determining and adsorption at Brønsted-acid

DOI: 10.1021/acs.jpcc.6b09703
J. Phys. Chem. C 2017, 121, 1618−1638

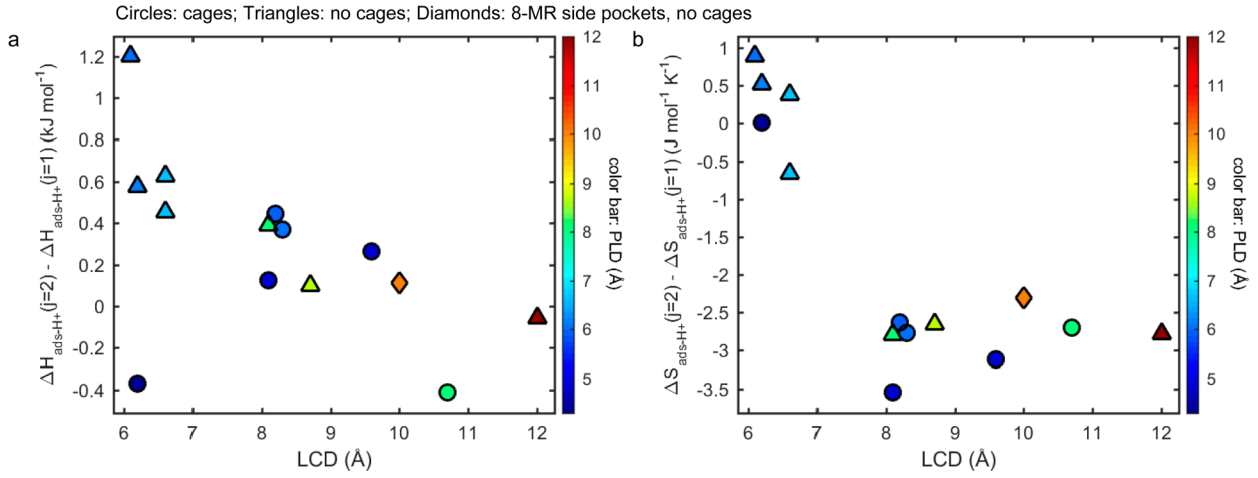

Figure 17. Difference in (a) enthalpy and (b) entropy of adsorption for *n*-butane, a reactant state via a central C−C bond ($j = 2$) vs a terminal C−C bond ($j = 1$) at 773 K for 1D zeolites with and without cages. The color bar indicates the pore-limiting diameter (PLD) given in Table 4.

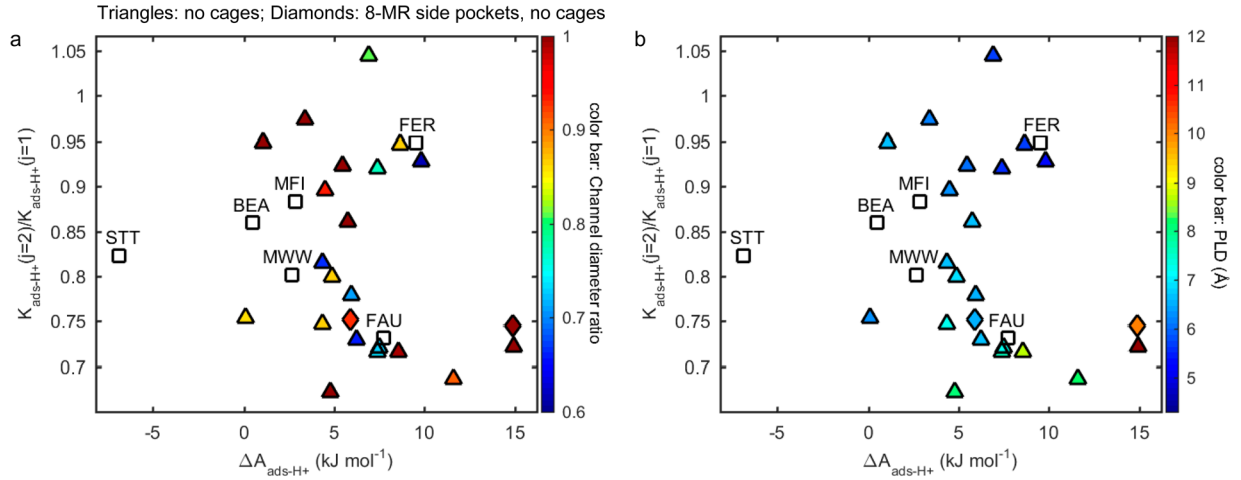

Figure 18. Ratio of the equilibrium constant for adsorption of *n*-butane via a central C−C bond ($j = 2$) to that for adsorption via a terminal C−C bond ($j = 1$) at 773 K for 1D zeolites without cages, vs the Helmholtz energy of adsorption. The color bars indicate (a) the ratio of the minimum to maximum channel width and (b) the pore-limiting diameter (PLD), given in Table 2.

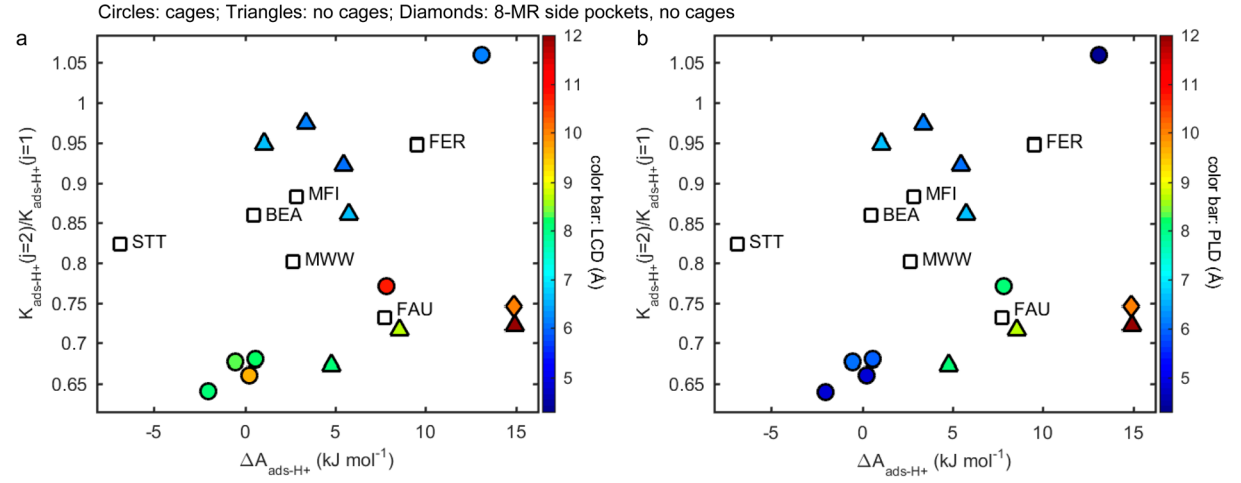

Figure 19. Ratio of the equilibrium constant for adsorption of *n*-butane via a central C−C bond ($j = 2$) to that for adsorption via a terminal C−C bond ($j = 1$) at 773 K for 1D zeolites with and without cages and having circular pores, vs the Helmholtz energy of adsorption. The color bars indicate (a) the largest cavity diameter (LCD) and (b) the pore-limiting diameter (PLD), given in Table 4.

sites can be considered to be quasi-equilibrated, leading to the following expression for the apparent first-order rate coefficient[34]

DOI: 10.1021/acs.jpcc.6b09703
J. Phys. Chem. C 2017, 121, 1618−1638

Table 5. IZA Framework Types and Material Names (in Parentheses), Pore-Limiting Diameter (PLD), Channel Diameters and Ratio of Channel Diameters, Largest Cavity Diameter (LCD), and Percentage of Pore Volume in the Cages

	properties taken from the IZA database			properties taken from ZEOMICS[b]		
framework type, material name,[a] dimensionality	ring size (T atoms)	diameter (Å)	diameter ratio[b] (Å)	PLD[b] (Å)	LCD[b] (Å)	% pore volume in cages[c]
BEA (Beta polymorph A), 3D	12	5.6 × 5.6	1.00	6.7	6.9	0
	12	7.7 × 6.6	0.86			
FAU (Faujasite), 3D	12	7.4 × 7.4	1.00	6.7	11.9	77
FER (Ferrierite), 2D	8	3.5 × 4.8	0.73	5.3	7.0	47
	10	4.2 × 5.4	0.78			
MFI (ZSM-5), 3D	10	5.1 × 5.5	0.93	5.0	7.0	26
	10	5.3 × 5.6	0.95			
MWW (SSZ-25), 2D	10	4.0 × 5.5	0.73	5.2	10.3	27
		4.1 × 5.1	0.80			
STT (SSZ-23), 1D	9	3.7 × 5.3	0.70	4.4	7.7	79

[a]Material names are in parentheses. Dimensionalities of the channel systems are taken from the IZA database. [b]Ratio of minimum to maximum diameter. [c]Pore-limiting diameter (PLD), largest cavity diameter (LCD), and percentage of pore volume in accessible cages obtained using the ZEOMICS web tool.[48]

$$k_{app}(j) = \frac{V_{H^+}}{RT} k_{int}(j) K_{ads\text{-}H^+}(j) = \frac{\nu_{H^+}}{h} \exp\left(-\frac{\Delta A_{ads\text{-}H^+}(j) + \Delta G^{\ddagger}_{int}(j)}{RT}\right) \quad (3)$$

where k_{int} is the intrinsic rate coefficient, $\Delta G^{\ddagger}_{int}$ is the intrinsic Gibbs free energy of activation, and the volume of a single reactant-state sphere of radius 5 Å is given by ν_{H^+}. As in sections 3.1 and 3.2, j denotes the bond to be cleaved, and values of 1 and 2 correspond to terminal and central cracking, respectively. (It is noted that the rate and selectivity to dehydrogenation are strongly correlated with the rate of terminal cracking and the ratio $k_{int}(j2)/k_{int}(j1)$, respectively.[34] Dehydrogenation is thus omitted from this analysis for conciseness.)

Equation 3 shows that the most active zeolite for central cracking will have the most favorable values of $\Delta A_{ads\text{-}H^+}(j2)$ and $\Delta G^{\ddagger}_{int}(j2)$, and the most selective zeolites will have the highest values for $K_{ads\text{-}H^+}(j2)/K_{ads\text{-}H^+}(j1)$ and the ratio $k_{int}(j2)/k_{int}(j1)$. To identify zeolites that are the best candidates for central cracking based on adsorption thermodynamics, plots of $K_{ads\text{-}H^+}(j2)/K_{ads\text{-}H^+}(j1)$ vs $\Delta A_{ads\text{-}H^+}$ are presented in Figures 18 and 19, respectively, for zeolites without cages and having different channel cross sections (discussed in section 3.1) and for zeolites with and without cages and having circular cross sections (discussed in section 3.2). Included on each plot are data calculated for commonly used multidimensional zeolites (FER, MFI, BEA, MWW, and FAU) and for STT, which was found to have the most favorable value of $\Delta A_{ads\text{-}H^+}$ out of all zeolites in the IZA database (none were found to have both a high value for $K_{ads\text{-}H^+}(j2)/K_{ads\text{-}H^+}(j1)$ and a value of $\Delta A_{ads\text{-}H^+}$ within the acceptable range). Topological data for these zeolites are included in Table 5.

It can be seen that none of the data are concentrated in the upper left corners of the plots, which is where the most desirable zeolites would appear. Figure 18 shows that, of the zeolites that lack cages, those with the smallest and largest PLDs tend to lie farthest from the upper left corners, and that PLDs of ∼6−7 Å and a diameter ratio of 1.00 appear to be optimal for the central cracking ($j2$) reactant state of n-butane. If the PLD is decreased, n-butane increasingly orients parallel to the channel, which promotes $j2$ adsorption but leads to repulsive contributions to $\Delta H_{ads\text{-}H^+}$. If the PLD is increased, n-butane orients increasingly perpendicular to the channel, promoting $j1$ adsorption and reducing enthalpic stabilization which increases $\Delta A_{ads\text{-}H^+}$ (see section 3.1). The two zeolites that exhibit an optimal balance between a favorable value for $\Delta A_{ads\text{-}H^+}$ and a favorable value for $K_{ads\text{-}H^+}(j2)/K_{ads\text{-}H^+}(j1)$ are CAN ($\Delta A_{ads\text{-}H^+}$ = 1.1 kJ mol^{-1}, $K_{ads\text{-}H^+}(j2)/K_{ads\text{-}H^+}(j1)$ = 0.95) and MRE ($\Delta A_{ads\text{-}H^+}$ = 3.4 kJ mol^{-1}, $K_{ads\text{-}H^+}(j2)/K_{ads\text{-}H^+}(j1)$ = 0.97), which lack cages and have PLDs of 6.6 and 6.2 Å, respectively. As shown in Figure 3 and Figure S.12, n-butane is centered within and tends to align parallel to the channel of CAN, maximizing van der Waals contacts and favoring $j2$ adsorption to a greater extent than in larger pores such as those of AFI (see Figure 8 and Figure S.14).

Figure 19 shows that none of the data for zeolites with cages fall near the data corresponding to the optimum zeolites (CAN and MRE). This observation is consistent with the finding, discussed in section 3.2, that zeolites with cages that can fully contain an alkane exhibit a favorable free energy of adsorption relative to zeolites with only channels at fixed PLD or at fixed LCD (Figure 15) but that such cages also promote free rotation and molecular configurations that favor terminal cracking reactant states. Thus, one-dimensional zeolites with cages large enough to contain n-butane fall within the bottom half of the plots and are not good candidates for central cracking based on a consideration of adsorption thermodynamics. Moreover, although intrinsic kinetic data are not available for nearly all of the zeolites investigated, based on recent experimental work,[34] the conclusions regarding the effect of cages at fixed PLD are expected to be even stronger if intrinsic kinetics are considered. The 1D zeolite TON (PLD 5.7 Å, see Table 1) was found to exhibit higher intrinsic and apparent rates and selectivity to central cracking vs terminal cracking relative to STF (PLD 6.0 Å, LCD 8.3 Å, see Table 3), which has a similar PLD but is comprised mostly of 8.3 Å cages (see Figure 14). Because of their lower confinement relative to channels, the cages were concluded to selectively stabilize terminal cracking and dehydrogenation transition states, thereby decreasing selectivity to central cracking relative to TON.

In addition, from the same work,[34] it was inferred that higher confinement, holding constant other structural parameters, promotes a higher rate and selectivity to central cracking. Extending this conclusion to the data for one-dimensional zeolites without cages presented in Figure 18, it seems likely that data in the upper right corners of the plots in Figure 18, which contain zeolites with the lowest PLDs, would become more desirable candidates for central cracking if intrinsic kinetics were

DOI: 10.1021/acs.jpcc.6b09703
J. Phys. Chem. C 2017, 121, 1618−1638

also considered. For either set of zeolites investigated, a more informed evaluation of the suitability of zeolite candidates would be possible by examining instead the values of k_{app} and the ratios of k_{app} corresponding to different reaction pathways, parameters that are convolutions of adsorption thermodynamic and intrinsic activation parameters (see eq 3). The CBMC methodology described in the present work provides first steps toward screening for desirable structural parameters based on adsorption. Apparent rate parameters determined by combining CBMC methodology with quantum mechanics calculations, or by using QM to determine rate parameters directly, would enable better evaluation of zeolite candidates. Empirical relationships could also be derived from additional experimental work similar to that employed in ref 34.

Finally, to better identify the structural features that are associated with desirable values of $K_{ads\text{-}H^+}(j2)/K_{ads\text{-}H^+}(j1)$ and $\Delta A_{ads\text{-}H^+}$, descriptors of channel and cage topology that represent the geometries of these features more realistically than do simple descriptors such as PLD and LCD are essential. Better descriptors for cage and channel dimensions, and different types of descriptors for more complex and multidimensional zeolite topologies, will help extend systematic analyses of the type performed here for simple 1D topologies to a greater range of structures, including those within the database of hypothetical zeolite structures. As noted, no data falling within the optimal regions of Figures 18 and 19 were obtained from CBMC simulations for zeolites listed within the IZA database. STT has been included because it exhibits the most negative value of $\Delta A_{ads\text{-}H^+}$ for *n*-butane of all zeolites in the database and, given a finding of favorable intrinsic kinetics, would be a suitable candidate for central cracking. CBMC simulations of zeolites contained in the database of hypothetical structures[56] would both build upon the conclusions from the present work and may reveal zeolite candidates that fall within the optimal regions of the plots.

4. CONCLUSIONS

The effects of zeolite framework topology on adsorption thermodynamics for *n*-alkanes adsorbed at Brønsted protons were systematically interpreted on the basis of quantified descriptors of pore topology. Attention was focused on *n*-butane adsorption within one-dimensional frameworks included in the IZA database. The enthalpy and entropy of adsorption ($\Delta H_{ads\text{-}H^+}$ and $\Delta S_{ads\text{-}H^+}$) at a fixed pore-limiting diameter (PLD)[48] generally decrease as the ratio of the minimum to maximum channel diameter increases, and are most negative for symmetric channels (for which the diameter ratio is equal to 1) as a result of the smaller cross-sectional area of such pores. In general, the free energy of adsorption, $\Delta A_{ads\text{-}H^+}$, is minimized for PLDs between 6 and 7 Å, and changes in this parameter with PLD are controlled by changes in $\Delta H_{ads\text{-}H^+}$ for PLDs larger than 6 Å. Changes in the diameter ratio do not result in systematic variation in $\Delta A_{ads\text{-}H^+}$ at 773 K. The preference for alkanes to adsorb onto active sites via a central vs a terminal C−C bond decreases as the PLD increases, until the PLD and alkane length become equal, as a result of increased rotational freedom and a tendency of the alkane to orient perpendicular to the channel direction. Further increases in PLD result in only weak changes to the adsorption selectivity because the alkane interacts increasingly with only one side of the channel.

The addition of cages larger in diameter than the PLD to a zeolite that has only channels decreases the magnitudes of both $\Delta H_{ads\text{-}H^+}$ and $\Delta S_{ads\text{-}H^+}$ because doing so decreases confinement. The replacement of channels of a given PLD with cages of the same diameter does not significantly affect $\Delta S_{ads\text{-}H^+}$, provided that the diameter is at least equal to the length of the *n*-alkane, because similar motion for the alkane is possible in both environments. However, $\Delta H_{ads\text{-}H^+}$ and $\Delta A_{ads\text{-}H^+}$ are lower in cages due to their greater curvature and surface area. As a result, the value of $\Delta A_{ads\text{-}H^+}$ for *n*-butane for zeolites with cages is minimized near ∼8 Å, which is nearly equal to the gas-phase gyration diameter of *n*-butane. The larger radius of the optimum cage (8 Å) vs that of the optimum channel (6−7 Å) for zeolites without cages suggests that cages promote greater van der Waals contacts with *n*-butane than do channels at a given dimension. The optimum cage size also appears to increase with the alkane length, providing direction for designing zeolites that selectively adsorb one alkane over another. The dependence on LCD of the selectivity to central C−C adsorption in zeolites with cages is very similar to the dependence on PLD observed for zeolites without cages for diameters less than the alkane length. For larger LCDs, the selectivity to adsorption via a central bond is generally lower for zeolites with cages because the cages better stabilize a freely rotating alkane and, therefore, selectively promote contact of the terminal bond with the cage wall.

The one-dimensional zeolites and other zeolites from the IZA database were also assessed with the objective of identifying structural features that enhance the rate of central C−C cracking through strong and selective adsorption of *n*-butane via a central C−C bond. No zeolites contained in the IZA database were found to exhibit a highly favorable combination of adsorption free energy and selectivity. In general, for the zeolites investigated, the free energy of adsorption and the selectivity of the adsorption were closest to the favorable region for zeolites without cages and having circular channels 6.2−6.6 Å in diameter. Larger channels generally exhibit higher free energy because of reduced van der Waals contacts, as well as lower selectivity to central C−C adsorption, while smaller channels result in better adsorption selectivity but higher free energy because of repulsive interactions. One-dimensional zeolites with cages were not strong candidates in general because of their low selectivity to central cracking reactant states. To identify zeolites that exhibit more desirable combinations of adsorption strength and selectivity than was observed for IZA-tabulated structures, studying the database of hypothetical zeolites, which contains hundreds of thousands of structures, is suggested in order to explore a significantly broader materials space.

In order to perform such a study, it would be useful to first develop better and additional descriptors with which to explain the influence of topology on thermodynamics for a smaller number of zeolites. The information gained could be used to target zeolites in the hypothetical database for CBMC simulations aimed at discovering zeolites with specified adsorption properties. Examples of such structural parameters include dimensionality, tortuosity and length of channel segments, and dimensions based on a realistic approximation of the shape of a cage or channel. Simple descriptors such as PLD and LCD that approximate channels and cages as cylinders and spheres, respectively, were found to be generally useful for the present study of simple 1D zeolites. However, even with simple frameworks, these descriptors were found to be inadequate in fully characterizing pore topology and its effects on thermodynamics. For example, the largest cavity diameter (LCD)[48] does not appear to be useful for interpreting differences in adsorption behavior between LTL and zeolites that have the same LCD but only channels; the LTL cage does not represent a sphere, and its

DOI: 10.1021/acs.jpcc.6b09703
J. Phys. Chem. C 2017, 121, 1618−1638

dimensions are not consistent with the LCD. In addition, the symmetry of the channel cross section, and not simply the PLD, was found to correlate with adsorption enthalpy and entropy, further demonstrating the importance of properly describing the shape as well as the size of zeolite voids.

■ ASSOCIATED CONTENT

Supporting Information

The Supporting Information is available free of charge on the ACS Publications website at DOI: 10.1021/acs.jpcc.6b09703.

Effects of Al content on adsorption thermodynamics, adsorption thermodynamic data for *n*-butane adsorbed in zeolites with 8-MR side pockets, supplemental plots of adsorption thermodynamic parameters for n-alkanes, and heat maps of *n*-butane C atom distributions obtained using NVT simulations (PDF)

■ AUTHOR INFORMATION

Corresponding Authors

*E-mail: lin.2645@osu.edu.

*E-mail: bell@cchem.berkeley.edu.

ORCID

Amber Janda: 0000-0001-8545-448X

Bess Vlaisavljevich: 0000-0001-6065-0732

Berend Smit: 0000-0003-4653-8562

Li-Chiang Lin: 0000-0002-2821-9501

Alexis T. Bell: 0000-0002-5738-4645

Present Address

[⊥]Department of Chemical Engineering, Stanford University, Stanford, California 94305, United States.

Notes

The authors declare no competing financial interest.

■ ACKNOWLEDGMENTS

This work was carried out with financial support from Chevron Energy Technology Company. A.J. also acknowledges an NDSEG fellowship awarded by the American Society for Engineering Education. The CBMC simulations were carried out using resources of the Ohio Supercomputer Center[57] and of the National Energy Research Scientific Computing Center, a DOE Office of Science User Facility supported by the Office of Science of the U.S. Department of Energy (Contract DE-AC02-05CH11231).

■ REFERENCES

(1) Vermeiren, W.; Gilson, J.-P. Impact of Zeolites on the Petroleum and Petrochemical Industry. *Top. Catal.* **2009**, *52*, 1131−1161.

(2) Primo, A.; Garcia, H. Zeolites as Catalysts in Oil Refining. *Chem. Soc. Rev.* **2014**, *43*, 7548−7561.

(3) Marcilly, C. R. Where and How Shape Selectivity of Molecular Sieves Operates in Refining and Petrochemistry Catalytic Processes. *Top. Catal.* **2000**, *13*, 357−366.

(4) Corma, A. From Microporous to Mesoporous Molecular Sieve Materials and Their Use in Catalysis. *Chem. Rev.* **1997**, *97*, 2373−2419.

(5) Abrevaya, H. Unique Aspects of Mechanisms and Requirements for Zeolite Catalysis in Refining and Petrochemicals. In *Zeolites in Industrial Separation and Catalysis*; Kulprathipanja, S., Ed.; Wiley-VCH Verlag GmbH & Co. KGaA: Weinheim, Germany, 2010; pp 403−478.

(6) Schenk, M.; Smit, B.; Vlugt, T. J. H.; Maesen, T. L. M. *Angew. Chem., Int. Ed.* **2001**, *40*, 736−739.

(7) Schenk, M.; Calero, S.; Maesen, T. L. M.; van Benthem, L. L.; Verbeek, M. G.; Smit, B. *Angew. Chem., Int. Ed.* **2002**, *41*, 2499−2502.

(8) Kulprathipanja, S.; James, R. B. Overview in Zeolites Adsorptive Separation. In *Zeolites in Industrial Separation and Catalysis*; Kulprathipanja, S., Ed.; Wiley-VCH Verlag GmbH & Co. KGaA: Weinheim, Germany, 2010; pp 173−202.

(9) Sohn, S. W. Liquid Industrial Non-Aromatics Adsorptive Separations. In *Zeolites in Industrial Separation and Catalysis*; Kulprathipanja, S., Ed.; Wiley-VCH Verlag GmbH & Co. KGaA: Weinheim, Germany, 2010; pp 249−272.

(10) Calero Diaz, S. Modeling of Transport and Accessibility in Zeolites. In *Zeolites and Catalysis: Synthesis, Reactions and Applications*; Čejka, J., Corma, A., Zones, S. I., Eds.; Wiley-VCH Verlag GmbH & Co. KGaA: Weinheim, Germany, 2010; Vol. 2, pp 335−360.

(11) Smit, B.; Maesen, T. L. M. Molecular Simulations of Zeolites: Adsorption, Diffusion, and Shape Selectivity. *Chem. Rev.* **2008**, *108*, 4125−4184.

(12) Smit, B.; Maesen, T. L. M. Towards a Molecular Understanding of Shape Selectivity. *Nature* **2008**, *451*, 671−678.

(13) Dubbeldam, D.; Calero, S.; Maesen, T. L. M.; Smit, B. Understanding the Window Effect in Zeolite Catalysis. *Angew. Chem., Int. Ed.* **2003**, *42*, 3624−3626.

(14) Maesen, T. L. M.; Beerdsen, E.; Calero, S.; Dubbeldam, D.; Smit, B. Understanding Cage Effects in the n-Alkane Conversion on Zeolites. *J. Catal.* **2006**, *237*, 278−290.

(15) Rigutto, M. Cracking and Hydrocracking. In *Zeolites and Catalysis: Synthesis, Reactions and Applications*; Čejka, J., Corma, A., Zones, S. I., Eds.; Wiley-VCH Verlag GmbH & Co. KGaA: Weinheim, Germany, 2010; Vol. 2, pp 547−584.

(16) Eder, F.; Lercher, J. A. Alkane Sorption in Molecular Sieves: The Contribution of Ordering, Intermolecular Interactions, and Sorption on Brønsted Acid Sites. *Zeolites* **1997**, *18*, 75−81.

(17) Eder, F.; Stockenhuber, M.; Lercher, J. A. Brønsted Acid Site and Pore Controlled Siting of Alkane Sorption in Acidic Molecular Sieves. *J. Phys. Chem. B* **1997**, *101*, 5414−5419.

(18) Denayer, J. F.; Baron, G. V.; Martens, J. A.; Jacobs, P. A. Chromatographic Study of Adsorption of n-Alkanes on Zeolites at High Temperatures. *J. Phys. Chem. B* **1998**, *102*, 3077−3081.

(19) Titiloye, J. O.; Parker, S. C.; Stone, F. S.; Catlow, C. R. A. Simulation Studies of the Structure and Energetics of Sorbed Molecules in High-Silica Zeolites. 1. Hydrocarbons. *J. Phys. Chem.* **1991**, *95*, 4038−4044.

(20) Smit, B.; Siepmann, J. I. Computer Simulations of the Energetics and Siting of n-Alkanes in Zeolites. *J. Phys. Chem.* **1994**, *98*, 8442−8452.

(21) June, L. R.; Bell, A. T.; Theodorou, D. N. Prediction of Low Occupancy Sorption of Alkanes in Silicalite. *J. Phys. Chem.* **1990**, *94*, 1508−1516.

(22) Bates, S. P.; van Well, W. J. M.; van Santen, R. A.; Smit, B. Configurational-Bias Monte Carlo (CB-MC) Calculations of n-Alkane Sorption in Zeolites RHO and FER. *Mol. Simul.* **1997**, *19*, 301−318.

(23) Denayer, J. F. M.; Ocakoglu, R. A.; Thybaut, J.; Marin, G.; Jacobs, P.; Martens, J.; Baron, G. V. n- and Isoalkane Adsorption Mechanisms on Zeolite MCM-22. *J. Phys. Chem. B* **2006**, *110*, 8551−8558.

(24) Denayer, J. F. M.; Ocakoglu, R. A.; Arik, I. C.; Kirschhock, C. E. A.; Martens, J. A.; Baron, G. V. Rotational Entropy Driven Separation of Alkane/Isoalkane Mixtures in Zeolite Cages. *Angew. Chem.* **2005**, *117*, 404−407.

(25) Luna-Triguero, A.; Vicent-Luna, J. M.; Dubbeldam, D.; Gómez-Álvarez, P.; Calero, S. Understanding and Exploiting Window Effects for Adsorption and Separations of Hydrocarbons. *J. Phys. Chem. C* **2015**, *119*, 19236−19243.

(26) Eder, F.; Lercher, J. A. On the Role of the Pore Size and Tortuosity for Sorption of Alkanes in Molecular Sieves. *J. Phys. Chem. B* **1997**, *101*, 1273−1278.

(27) Savitz, S.; Siperstein, F.; Gorte, R. J.; Myers, A. L. Calorimetric Study of Adsorption of Alkanes in High Silica Zeolites. *J. Phys. Chem. B* **1998**, *102*, 6865−6872.

(28) Gribov, E. N.; Sastre, G.; Corma, A. Influence of Pore Dimension and Sorption Configuration on the Heat of Sorption of Hexane on Monodimensional Siliceous Zeolites. *J. Phys. Chem. B* **2005**, *109*, 23794−23803.

(29) Bates, S. P.; van Well, W. J. M.; van Santen, R. A.; Smit, B. Energetics of n-Alkanes in Zeolites: A Configurational-Bias Monte Carlo Investigation into Pore Size Dependence. *J. Am. Chem. Soc.* **1996**, *118*, 6753−6759.
(30) Bučko, T.; Hafner, J. The Role of Spatial Constraints and Entropy in the Adsorption and Transformation of Hydrocarbons Catalyzed by Zeolites. *J. Catal.* **2015**, *329*, 32−48.
(31) Bučko, T.; Benco, L.; Hafner, J.; Ángyán, J. G. Monomolecular Cracking of Propane over Acidic Chabazite: An Ab Initio Molecular Dynamics and Transition Path Sampling Study. *J. Catal.* **2011**, *279*, 220−228.
(32) Jiang, T.; Göltl, F.; Bulo, R. E.; Sautet, P. Effect of Temperature on the Adsorption of Short Alkanes in the Zeolite SSZ-13: Adapting Adsorption Isotherms to Microporous Materials. *ACS Catal.* **2014**, *4*, 2351−2358.
(33) Janda, A.; Vlaisavljevich, B.; Lin, L.-C.; Sharada, M. S.; Smit, B.; Head-Gordon, M.; Bell, A. T. Adsorption Thermodynamics and Intrinsic Activation Parameters for Monomolecular Cracking of n-Alkanes on Brønsted Acid Sites in Zeolites. *J. Phys. Chem. C* **2015**, *119*, 10427−10438.
(34) Janda, A.; Lin, L.-C.; Vlaisavljevich, B.; Smit, B.; Bell, A. T. Effects of Zeolite Structural Confinement on Adsorption Thermodynamics and Reaction Kinetics for Monomolecular Cracking and Dehydrogenation of n-Butane. *J. Am. Chem. Soc.* **2016**, *138*, 4739−4756.
(35) De Moor, B. A.; Ghysels, A.; Reyniers, M.-F.; Van Speybroeck, V.; Waroquier, M.; Marin, G. B. Normal Mode Analysis in Zeolites: Toward an Efficient Calculation of Adsorption Entropies. *J. Chem. Theory Comput.* **2011**, *7*, 1090−1101.
(36) De Moor, B. A.; Reyniers, M.-F.; Gobin, O. C.; Lercher, J. A.; Marin, G. B. Adsorption of C2-C8 n-Alkanes in Zeolites. *J. Phys. Chem. C* **2011**, *115*, 1204−1219.
(37) Swisher, J. A.; Hansen, N.; Maesen, T.; Keil, F. J.; Smit, B.; Bell, A. T. Theoretical Simulation of n-Alkane Cracking on Zeolites. *J. Phys. Chem. C* **2010**, *114*, 10229−10239.
(38) Frenkel, D.; Smit, B. Free Energy Calculations. *Understanding Molecular Simulation: From Algorithms to Applications*, 2nd ed.; Computational Science Series, Vol *1*; Academic Press: New York, 2001; pp 173−176.
(39) Dubbeldam, D.; Calero, S.; Vlugt, T. J. H.; Krishna, R.; Maesen, T. L. M.; Beerdsen, E.; Smit, B. Force Field Parametrization through Fitting on Inflection Points in Isotherms. *Phys. Rev. Lett.* **2004**, *93*, No. 088302.
(40) Willems, T. F.; Rycroft, C. H.; Kazi, M.; Meza, J. C.; Haranczyk, M. Algorithms and Tools for High-Throughput Geometry-Based Analysis of Crystalline Porous Materials. *Microporous Mesoporous Mater.* **2012**, *149*, 134−141.
(41) Myers, A. L.; Monson, P. A. Physical Adsorption of Gases: The Case for Absolute Adsorption as the Basis for Thermodynamic Analysis. *Adsorption* **2014**, *20*, 591−622.
(42) Eilers, P. H. C.; Goeman, J. J. Enhancing Scatterplots with Smoothed Densities. *Bioinformatics* **2004**, *20*, 623−628.
(43) June, L. R.; Bell, A. T.; Theodorou, D. N. Molecular Dynamics Studies of Butane and Hexane in Silicalite. *J. Phys. Chem.* **1992**, *96*, 1051−1060.
(44) Nicholas, J. B.; Trouw, F. R.; Mertz, J. E.; Iton, L. E.; Hopfinger, A. J. Molecular Dynamics Simulation of Propane and Methane in Silicalite. *J. Phys. Chem.* **1993**, *97*, 4149−4163.
(45) Fujiyama, S.; Seino, S.; Kamiya, N.; Nishi, K.; Yoza, K.; Yokomori, Y. Adsorption Structures of Non-Aromatic Hydrocarbons on Silicalite-1 Using the Single-Crystal X-Ray Diffraction Method. *Phys. Chem. Chem. Phys.* **2014**, *16*, 15839−15845.
(46) Derycke, I.; Vigneron, J. P.; Lambin, P.; Lucas, A. A.; Derouane, E. G. Physisorption in Confined Geometry. *J. Chem. Phys.* **1991**, *94*, 4620−4627.
(47) Derouane, E. G.; Andre, J.-M.; Lucas, A. A. Surface Curvature Effects in Physisorption and Catalysis by Microporous Solids and Molecular Sieves. *J. Catal.* **1988**, *110*, 58−73.
(48) First, E. L.; Gounaris, C. E.; Wei, J.; Floudas, C. A. Computational Characterization of Zeolite Porous Networks: An Automated Approach. *Phys. Chem. Chem. Phys.* **2011**, *13*, 17339−17358.
(49) Snyder, P. W.; Lockett, M. R.; Moustakas, D. T.; Whitesides, G. M. Is it the Shape of the Cavity, or the Shape of the Water in the Cavity? *Eur. Phys. J.: Spec. Top.* **2014**, *223*, 853−891.
(50) Gallicchio, E.; Kubo, M.; Levy, R. M. Entropy-Enthalpy Compensation in Solvation and Ligand Binding Revisited. *J. Am. Chem. Soc.* **1998**, *120*, 4526−4527.
(51) Ryde, U. A Fundamental View of Enthalpy-Entropy Compensation. *MedChemComm* **2014**, *5*, 1324−1336.
(52) Gounder, R.; Iglesia, E. The Roles of Entropy and Enthalpy in Stabilizing Ion-Pairs at Transition States in Zeolite Acid Catalysis. *Acc. Chem. Res.* **2012**, *45*, 229−238.
(53) Broach, R. W. Zeolite Types and Structures. In *Zeolites in Industrial Separation and Catalysis*; Kulprathipanja, S., Ed.; Wiley-VCH Verlag GmbH & Co. KGaA: Weinheim, Germany, 2010; pp 27−59.
(54) Breck, D. W. *Zeolite Molecular Sieves: Structure, Chemistry and Use*; Wiley: New York, 1973.
(55) Schmeits, M.; Lucas, A. A. Physical Adsorption and Surface Plasmons. *Surf. Sci.* **1977**, *64*, 176−196.
(56) Deem, M. W.; Pophale, R.; Cheeseman, P. A.; Earl, D. Computational Discovery of New Zeolite-Like Materials. *J. Phys. Chem. C* **2009**, *113*, 21353−21360.
(57) Ohio Supercomputer Center, http://osc.edu/ark:/19495/f5s1ph73, 1987.

DOI: 10.1021/acs.jpcc.6b09703
J. Phys. Chem. C 2017, 121, 1618−1638